

1      **Response to interactive comments on “The tropical tropopause  
2      layer in reanalysis data sets” by Tegtmeier et al.**

3

4      We thank the reviewer for his/her comments which have helped us to improve the paper in  
5      revision. Comments are reproduced below, followed by our responses in *italics*. Changes to  
6      the manuscript are marked in blue bold print.

7

8      **Anonymous Referee #2**

9

10     I wish to thank the authors to have considered my previous comments and to have addressed  
11    them positively. I still have two (minor) comments and I suggest publishing the paper after  
12    having considered them.

13

14     1. The reanalyses discussed in this paper are introduced too far away (in Sect. 2.2). Their  
15    acronyms are also undefined. I suggest to introduce the reanalyses in the introduction (including  
16    the definition of the acronym) and, possibly also, in the abstract. In the abstract, I would also  
17    provide the name of the reanalyses concerned by “most recent atmospheric reanalysis ...”  
18    (P2L12).

19

20     *We have added a list of the reanalyses discussed in the paper to the introduction and  
21    abstract. Acronyms are defined in section 2.2.*

22

23     2. According to Sherwood (2000, GRL), the “maritime continent” corresponds to the general  
24    area of Indonesia. I thus suggest to replace (P15L5) “... “maritime continent”... ” by “...  
25    “maritime continent” (i.e. the general area of Indonesia)...”.

26

27     *We have added the suggested specification to the text.*

1      **Temperature and tropopause characteristics from**  
2      **reanalyses data in the tropical tropopause layer**

4      Susann Tegtmeier<sup>1\*</sup>, James Anstey<sup>2</sup>, Sean Davis<sup>3</sup>, Rossana Dragani<sup>4</sup>, Yayoi Harada<sup>5</sup>, Ioana  
5      Ivanciu<sup>1</sup>, Robin Pilch Kedzierski<sup>1</sup>, Kirstin Krüger<sup>6</sup>, Bernard Legras<sup>7</sup>, Craig Long<sup>8</sup>, James S.  
6      Wang<sup>9</sup>, Krzysztof Wargan<sup>10,11</sup>, and Jonathon S. Wright<sup>12</sup>

10     <sup>1</sup>GEOMAR Helmholtz Centre for Ocean Research Kiel, 24105 Kiel, Germany

11     **\*now at Institute of Space and Atmospheric Studies, University of Saskatchewan,**  
12     **Saskatoon, Canada**

13     <sup>2</sup>Canadian Centre for Climate Modelling and Analysis, ECCC, Victoria, Canada

14     <sup>3</sup>Earth System Research Laboratory, National Oceanic and Atmospheric Administration,  
15     Boulder, CO 80305, USA

16     <sup>4</sup>European Centre for Medium-Range Weather Forecasts, Reading, RG2 9AX, UK

17     <sup>5</sup>Japan Meteorological Agency, Tokyo, 100-8122, Japan

18     <sup>6</sup> Section for Meteorology and Oceanography, Department of Geosciences, University of Oslo,  
19     0315 Oslo, Norway

20     <sup>7</sup>Laboratoire de Météorologie Dynamique, CNRS/PSL-ENS, Sorbonne University Ecole  
21     Polytechnique, France

22     <sup>8</sup>Climate Prediction Center, National Centers for Environmental Prediction, National Oceanic  
23     and Atmospheric Administration, College Park, MD 20740, USA

24     <sup>9</sup>Institute for Advanced Sustainability Studies, Potsdam, Germany

25     <sup>10</sup>Science Systems and Applications, Inc., Lanham, MD 20706, USA

26     <sup>11</sup>Global Modeling and Assimilation Office, Code 610.1, NASA Goddard Space Flight  
27     Center, Greenbelt, MD 20771, USA

28     <sup>12</sup>Department of Earth System Science, Tsinghua University, Beijing, 100084, China

29

30

31

32

33

34

35

36

1    **Abstract**

2  
3    The tropical tropopause layer (TTL) is the transition region between the well mixed, convective  
4    troposphere and the radiatively controlled stratosphere with air masses showing chemical and  
5    dynamical properties of both regions. The representation of the TTL in meteorological  
6    reanalysis data sets is important for studying the complex interactions of circulation,  
7    convection, trace gases, clouds and radiation. In this paper, we present the evaluation of  
8    climatological and long-term TTL temperature and tropopause characteristics in the reanalysis  
9    data sets **ERA-Interim, ERA5, JRA-25, JRA-55, MERRA, MERRA-2, NCEP-NCAR R1, and CFSR**. The evaluation has been performed as part of the SPARC (Stratosphere–  
10   troposphere Processes and their Role in Climate) Reanalysis Intercomparison Project (S-RIP).

11  
12  
13    The most recent atmospheric reanalysis data sets (**ERA-Interim, ERA5, JRA-55, MERRA-2, and CFSR**) all provide realistic representations of the major characteristics of the  
14    temperature structure within the TTL. There is good agreement between reanalysis estimates  
15    of tropical mean temperatures and radio occultation data, with relatively small cold biases for  
16    most data sets. Temperatures at the cold point and lapse rate tropopause levels, on the other  
17    hand, show warm biases in reanalyses when compared to observations. This tropopause-level  
18    warm bias is related to the vertical resolution of the reanalysis data, with the smallest bias found  
19    for data sets with the highest vertical resolution around the tropopause. Differences of the cold  
20    point temperature maximise over equatorial Africa, related to Kelvin wave activity and  
21    associated disturbances in TTL temperatures.

22  
23    Interannual variability in reanalysis temperatures is best constrained in the upper TTL, with  
24    larger differences at levels below the cold point. The reanalyses reproduce the temperature  
25    responses to major dynamical and radiative signals such as volcanic eruptions and the QBO.  
26    Long-term reanalysis trends in temperature in the upper TTL show good agreement with trends  
27    derived from adjusted radiosonde data sets indicating significant stratospheric cooling of  
28    around  $-0.5$  to  $-1$  K/decade. At 100 hPa and the cold point, most of the reanalyses suggest small  
29    but significant cooling trends of  $-0.3$  to  $-0.6$  K/decade that are statistically consistent with  
30    trends based on the adjusted radiosonde data sets.

31  
32    Advances of the reanalysis and observational systems over the last decades have led to a clear  
33    improvement of the TTL reanalyses products over time. Biases of the temperature profiles and  
34    differences in interannual variability clearly decreased in 2006, when densely sampled radio  
35    occultation data started being assimilated by the reanalyses. While there is an overall good  
36    agreement, different reanalyses offer different advantages in the TTL such as realistic profile  
37    and cold point temperature, continuous time series or a realistic representation of signals of  
38    interannual variability. Their use in model simulations and in comparisons with climate model  
39    output should be tailored to their specific strengths and weaknesses.

40

41

42

43

1    **1. Introduction**

2  
3    The tropical tropopause layer (TTL) is the transition region between the well-mixed, convective  
4    troposphere and the radiatively-controlled stratosphere. The vertical range of the TTL extends  
5    from the region of strong convective outflow near 12-14 km to the highest altitudes reached by  
6    convective overshooting events, around 18 km (Highwood and Hoskins, 1998; Folkins et al  
7    1999; Fueglistaler et al., 2009; Randel and Jensen, 2013). Air masses in the TTL show  
8    dynamical and chemical properties of both the troposphere and the stratosphere, and are  
9    controlled by numerous processes on a wide range of length and time scales. Complex  
10   interactions among circulation, convection, trace gases, clouds and radiation in the TTL make  
11   this region a key player in radiative forcing and chemistry-climate coupling. As the TTL is the  
12   main gateway for air entering the stratosphere, stratospheric chemistry and composition, and  
13   especially the abundances of ozone, water vapour and aerosols, are strongly impacted by the  
14   properties of air near the tropical tropopause (e.g., Mote et al., 1996; Holton and Gettelman,  
15   2001; Fueglistaler et al., 2011).

16  
17   The tropopause is the most important physical boundary within the TTL, serving to separate  
18   the turbulent, moist troposphere from the stable, dry stratosphere. The position of the  
19   tropopause is determined by the thermal properties of the TTL, as a negative, tropospheric  
20   vertical temperature gradient changes into a positive stratospheric temperature gradient. The  
21   role of the tropopause as a physical boundary is evident not only from the vertical temperature  
22   structure, but also from the distributions of atmospheric trace gases and clouds (Pan and  
23   Munchak, 2011; Pan et al., 2018).

24  
25   In the tropics, two definitions of the tropopause are widely used: one based on the cold point  
26   and one based on the characteristics of the lapse rate. The cold point tropopause is defined as  
27   the level at which the vertical temperature profile reaches its minimum (Highwood and Hoskins,  
28   1998) and air parcels en route from the troposphere to the stratosphere encounter the lowest  
29   temperatures. Final dehydration typically occurs at these lowest temperatures, so that the cold  
30   point tropopause effectively controls the overall water vapour content of the lower stratosphere  
31   (Randel et al., 2004a) and explains its variability (Fueglistaler et al., 2009). While the cold point  
32   tropopause is an important boundary in the tropics where upwelling predominates, this  
33   definition of the tropopause is irrelevant for water vapor transport into the stratosphere at higher  
34   latitudes. The lapse rate tropopause, on the other hand, offers a globally-applicable definition  
35   of the tropopause, marking a vertical discontinuity in the static stability. The lapse rate  
36   tropopause is defined as the lowest level at which the lapse rate decreases to  $2 \text{ K km}^{-1}$  or less,  
37   provided that the average lapse rate between this level and all higher levels within 2 km does  
38   not exceed  $2 \text{ K km}^{-1}$  (World Meteorological Organization, 1957). The tropical lapse rate  
39   tropopause is typically  $\sim 0.5 \text{ km}$  ( $\sim 7 \text{ hPa}$ ) lower and  $\sim 1 \text{ K}$  warmer than the cold point tropopause  
40   (Seidel et al., 2001).

41  
42   Over recent decades, the thermal characteristics of the TTL and tropopause have been obtained  
43   from tropical radiosonde and Global Navigation Satellite System - Radio Occultation (GNSS-  
44   RO) upper air measurements. Radiosonde profiles offer temperature, wind and air pressure data  
45   at a high vertical resolution. However, climate records based on radiosonde data often suffer

1 from spatial inhomogeneities or time-varying biases due to changes in instruments and  
2 measurement practices (Seidel and Randel, 2006; Wang et al., 2012). Climate records from  
3 radio occultation data offer much better spatial coverage and density, but are only available  
4 starting from 2002. As a result, studies of long-term variability and trends in TTL and  
5 tropopause properties have also used reanalysis data (e.g., Santer et al., 2003; Gettelman et al.,  
6 2010, Xie et al., 2014).

7  
8 Meteorological reanalysis data sets are widely used in scientific studies of atmospheric  
9 processes and variability, either as initial conditions for historical model runs or in comparisons  
10 with climate model output. Often, they are utilized as “stand-ins” for observations, when the  
11 available measurements lack the spatial or temporal coverage needed. Each atmospheric  
12 reanalysis system consists of a fixed global forecast model and assimilation scheme. The system  
13 combines short-range forecasts of the atmospheric state with available observations to produce  
14 best-guess, consistent estimates of atmospheric variables such as temperatures and winds.  
15 Spurious changes in the reanalysis fields can arise from changes in the quality and quantity of  
16 the observations used as input data, which complicates the analysis of variability and trends.  
17 Further discontinuities in reanalysis-based time series can originate from the joining together  
18 of distinct execution streams (Fujiwara et al., 2017).

19  
20 Among the various TTL characteristics such as composition, radiation budgets and cloud  
21 properties, the vertical temperature structure and the position and temperature of the cold point  
22 are of particular importance for transport and composition studies. Many off-line chemistry-  
23 transport models or Lagrangian particle dispersion models are driven by reanalysis data sets  
24 (e.g., Chipperfield, 1999; Krüger et al., 2009; Schoeberl et al., 2012; Tao et al., 2019). Their  
25 representation of the cold point determines how realistically such models simulate dehydration  
26 and stratospheric entrainment processes. Process studies of TTL dynamics such as equatorial  
27 wave variability are also often based on the TTL temperature structure in reanalysis data sets  
28 (e.g., Fujiwara et al., 2012). Finally, reanalysis cold point temperature and height have been  
29 used in the past for comparison to model results and in investigations of long-term changes  
30 (e.g., Gettelman et al., 2010). Information on the quality and biases of TTL temperature and  
31 tropopause data are important for all above listed studies of transport, composition, dynamics  
32 and long-term changes of the TTL.

33  
34 A comparison of the reanalysis products available at the end of the 1990s (including ERA-15,  
35 ERA-40 and NCEP-NCAR R1) with other climatological datasets showed notable differences  
36 in temperatures near the tropical tropopause (Randel et al., 2004b). While the ECMWF  
37 reanalyses agreed relatively well with radiosonde observations at 100 hPa, NCEP-NCAR R1  
38 showed a warm bias of up to 3 K, probably resulting from low vertical resolution and the use  
39 of poorly-resolved satellite temperature retrievals (Fujiwara et al., 2017). Comparisons of  
40 winter temperatures at 100 hPa between more recent reanalyses, such as MERRA, NCEP CFSR  
41 and ERA-Interim, and Singapore radiosonde observations show better agreement, with  
42 reanalyses generally 1-2 K too cold at this level (Schoeberl et al., 2012). While many studies  
43 have highlighted the characteristics of individual reanalysis data sets, a comprehensive  
44 intercomparison of the TTL among all major atmospheric reanalyses is currently missing.

45

1 Here, we investigate whether the reanalysis data sets **ERA-Interim, ERA5, JRA-25, JRA-55, MERRA, MERRA-2, NCEP-NCAR (R1), and CFSR** reproduce key characteristics of the  
2 temperature and tropopauses in the TTL. This work has been conducted as part of the SPARC  
3 (Stratosphere–troposphere Processes and their Role in Climate) Reanalysis Intercomparison  
4 Project (S-RIP) (Fujiwara et al., 2017) and presents some of the key findings from the S-RIP  
5 report Chapter 8 on the TTL. Climatologies of the tropical cold point and lapse rate tropopauses  
6 as derived from modern reanalysis data sets are compared to high-resolution radio occultation  
7 data (Section 3). We also investigate temporal variability and long-term changes in tropopause  
8 levels and temperature within the TTL (Section 4). The observational and reanalysis data sets  
9 used in the evaluation are introduced in Section 2, and a discussion and summary of the results  
10 are provided in Section 5.

12

## 13 **2 Data and methods**

14

### 15 **2.1 Observational data sets**

16

17 Observations of the TTL temperatures are available from tropical radiosonde stations.  
18 However, climate records of radiosonde temperature, height and pressure data often suffer from  
19 inhomogeneities or time-varying biases due to changes in instruments or measurement practices  
20 (Seidel and Randel, 2006). Adjusted radiosonde temperature data sets at 100 hPa, 70 hPa and  
21 corresponding trends at the cold point have been created by removing such inhomogeneities  
22 (Wang et al., 2012, and references therein). In this chapter, we use the four independently  
23 adjusted radiosonde data sets RATPAC (Free et al., 2005), RAOBCORE (Haimberger, 2007),  
24 RICH (Haimberger et al., 2012) and HadAT (Thorne et al., 2005) for evaluations at 70 and 100  
25 hPa. The interannual anomalies at 70 hPa are shown only for RAOBCORE to improve the  
26 clarity of the figure, but all data sets are discussed in the text. For trends at 70 and 100 hPa, we  
27 show the smallest and largest trends derived from the four adjusted radiosonde data sets as  
28 reported by Wang et al. (2012) and consider their range (including error bars) as the  
29 observational uncertainty range.

30

31 Evaluations of the interannual anomalies of cold point temperature, height and pressure are  
32 based on the unadjusted, quality-controlled radiosonde data set IGRA (Durre et al., 2006) as  
33 temperature adjustments can change the location of the cold point in a profile. The trend of cold  
34 point temperature cannot be derived from the unadjusted IGRA data set due to inhomogeneities  
35 or time-varying biases caused by changes in instruments and measurement practices (see Wang  
36 et al., 2012 for a detailed discussion). Instead we use adjusted cold points derived from the  
adjusted radiosonde data sets discussed above.

37

38 Since 2002, high-resolution temperature and pressure data in the TTL are also available from  
39 satellite retrievals based on the GNSS-RO technique. Recent studies have demonstrated good  
40 agreement between GNSS-RO and radiosonde temperature profiles (e.g. Anthes et al., 2008;  
41 Ho et al., 2017). We use a monthly mean zonal mean data set constructed from measurements  
42 collected by the Challenging Minisat Payload (CHAMP, Wickert et al., 2001), Gravity  
43 Recovery and Climate Experiment (GRACE, Beyerle et al., 2005), Constellation Observing  
44 System for Meteorology, Ionosphere, and Climate (COSMIC, Anthes et al., 2008), Metop-A  
(von Engeln et al., 2011), Metop-B, Satélite de Aplicaciones Científicas-C/Scientific

1 Application Satellite-C (SAC-C, Hajj et al., 2004), and TerraSAR-X (Beyerle et al., 2011)  
2 missions. All data are re-processed or post-processed occultation profiles with moisture  
3 information ('wetPrf' product) as provided by the COSMIC Data Analysis and Archive Center  
4 (CDAAC, <https://cdaac-www.cosmic.ucar.edu/cdaac/products.html>). The GNSS-RO 'wetPrf'  
5 temperature profiles from CDAAC are provided on a 100-m vertical grid from the surface to  
6 40 km altitude. The effective physical resolution is variable, ranging from ~1 km in regions of  
7 constant stratification down to 100-200m where the biggest stratification gradients occur e.g.  
8 at the top of the boundary layer or at a very sharp tropopause (Kursinski et al., 1997; Gorbunov  
9 et al., 2004), most often being somewhere in between. The observational temperature records  
10 at reanalysis model levels in the TTL region have been determined by interpolating each GNSS-  
11 RO temperature profile to the reanalysis model levels with the barometric formula, taking into  
12 account the lapse rate between levels. For each profile, the cold point and lapse rate tropopause  
13 characteristics were identified based on the cold point and WMO criteria, respectively. Zonal  
14 and long-term averages of the tropopause metrics and temperatures at model levels are  
15 calculated by averaging over all grid points and represent the final step of data processing.

16 We also use a daily data set of cold point temperatures obtained from all GNSS-RO missions,  
17 gridded on a  $5^\circ \times 5^\circ$  grid between  $30^\circ\text{N}$  and  $30^\circ\text{S}$ . For each  $5^\circ$  wide latitude band, we apply a  
18 two-dimensional fast Fourier transform to detect Kelvin wave anomalies for planetary  
19 wavenumbers 1–15, periods of 4–30 days and equivalent depths of 6–600 following the  
20 theoretical dispersion curves for Kelvin waves as in Wheeler and Kiladis (1999). We allow a  
21 wider range of equivalent depths, since it has been shown that Kelvin waves tend to propagate  
22 faster around the tropical tropopause than they do in the troposphere (Kim and Son, 2012). The  
23 filtered anomalies represent cold point temperature variability that propagates in the same  
24 wavenumber-frequency domain as Kelvin waves, i.e. when the temperature is modulated by  
25 Kelvin waves present around the tropopause. The spatial variance of the filtered signals is used  
26 to calculate a monthly index as a measure of the amount of Kelvin wave activity in the TTL.  
27 The index is calculated as the  $1\sigma$  standard deviation over the filtered anomalies at all spatial  
28 grid points. Time periods of enhanced Kelvin wave activity are defined as the months when the  
29 index is larger than the long-term mean plus the  $1\sigma$  standard deviation of the whole time series.  
30 Based on this definition, we determined 20% of all months to be characterized by enhanced  
31 Kelvin wave activity.

32

## 33 2.2 Reanalysis data sets

34

35 We evaluate eight “full-input” reanalyses, where a full-input reanalysis is defined as a systems  
36 that assimilate surface and upper-air conventional and satellite data. In this paper, we focus on  
37 **the European Centre for Medium-Range Weather Forecasts (ECMWF) Interim**  
38 **Reanalysis** (ERA-Interim; Dee et al., 2011), **the forthcoming reanalysis developed by**  
39 **ECMWF** (ERA5; Hersbach et al., 2018), **the Japanese 25-year Reanalysis** (JRA-25; Onogi  
40 et al., 2007), **the Japanese 55-year Reanalysis** (JRA-55; Kobayashi et al., 2015), the **Modern**  
41 **Era Retrospective-Analysis for Research** (MERRA; Rienecker et al., 2011), the MERRA-2  
42 (Gelaro et al., 2017), **the National Centers for Environmental Prediction (NCEP) - National**  
43 **Center for Atmospheric Research (NCAR) Reanalysis 1** (NCEP-NCAR Reanalysis 1;

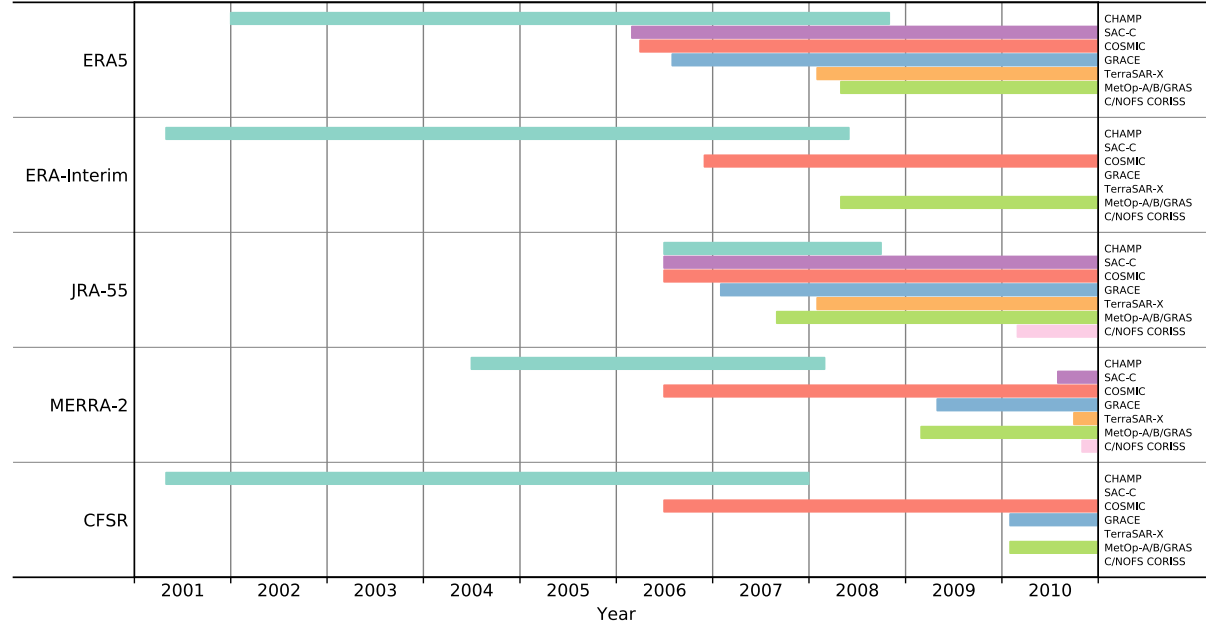
1 Kistler et al., 2001; referred to hereafter as R1), and **the Global Forecast System of the NCEP**  
2 **Reanalysis** (CFSR; Saha et al., 2010). We limit our analyses to the S-RIP core intercomparison  
3 period 1980–2010. Due to availability at the time of the evaluations, ERA5 is only evaluated  
4 over 2002–2010. Details of each reanalysis, including model characteristics, physical  
5 parameterizations, assimilated observations, execution streams, and assimilation strategies  
6 have been summarized by Fujiwara et al. (2017).

7 Global temperature fields in the reanalysis data sets are constrained by assimilating  
8 conventional (surface and balloon), aircraft, and satellite observations. The most important  
9 sources of assimilated data for stratospheric temperatures are the microwave and infrared  
10 satellite sounders of the TOVS suite (1979–2006) and the ATOVS suite (1998–present). All of  
11 the above reanalysis systems assimilate microwave and infrared radiances from these  
12 instruments, except for NCEP-NCAR R1 which assimilates temperature retrievals instead.  
13 Measurements from the ATOVS suite, which has a higher number of channels compared to  
14 TOVS, have been assimilated from about 1998, although the exact start dates differ among the  
15 reanalyses. The introduction of ATOVS considerably improved the vertical resolution of the  
16 assimilated data. Some of the reanalyses (ERA-Interim, ERA5, MERRA, MERRA-2, and  
17 CFSR) also assimilate radiances from the hyperspectral infrared sounders AIRS (2002–  
18 present), IASI (2008–present), and/or CrIS (2012–present), although the latter was not available  
19 for assimilation during the intercomparison period considered here. Because radiance biases  
20 associated with instrument changes, inaccurate calibration offsets, orbital drifts or long-term  
21 CO<sub>2</sub> changes can cause unwanted biases in the resulting reanalysis temperature fields (e.g.  
22 Rienecker et al., 2011), a variational bias correction scheme is used during the data assimilation  
23 procedure to remove or minimize any radiance biases. This ensures that any temperature  
24 changes introduced by the circumstances outlined above are kept small, which is important  
25 when looking for long term changes.

26 All full-input reanalyses assimilate upper-air temperature observations from radiosondes which  
27 are available at a very high vertical resolution. Systematic errors in radiosonde profiles caused  
28 by effects of solar radiative heating on the temperature sensor (Nash et al., 2011) have typically  
29 been corrected either onsite or at the reanalysis centre before assimilation (Fujiwara et al.,  
30 2017). In order to avoid discontinuities or inconsistencies in temperature time series from  
31 radiosondes, several reanalysis systems use homogenized temperature data sets such as  
32 RAOBCORE (ERA-Interim, JRA-55, MERRA, MERRA-2) and RICH (ERA5). Earlier  
33 reanalyses (ERA-40 and JRA-25) used simplified homogenization approaches that mostly  
34 corrected for daily and seasonal variations. Although the detailed quality control procedures for  
35 radiosonde and other conventional data imported from the global distribution network can vary  
36 among the individual reanalyses, the conventional data archives are often shared among the  
37 centres (see also Fujiwara et al., 2017).

38 Recent reanalysis systems have also included information from GNSS-RO instruments by  
39 assimilating observations of the bending angle up to 30 km (Cucurull et al., 2013). Assimilating  
40 these high vertical resolution data affects reanalysis temperature and provides an additional  
41 ‘anchor’ for adaptive bias correction of satellite radiances. JRA-55 assimilates refractivity  
42 profiles up to 30 km, which are functions of temperature, humidity, and pressure. For all recent  
43 reanalyses, the advent of the COSMIC mission in 2006 significantly increased the number of  
44 GNSS-RO profiles available for assimilation. Details of the various GNSS-RO data assimilated

1 by ERA5, ERA-Interim, JRA-55, MERRA-2 and CFSR up to the end of 2010 are listed in  
 2 **Table 1**. In addition to the GNSS-RO data sets discussed in section 2.1, C/NOFS-CORISS  
 3 (Communications/Navigation Outage Forecasting System Occultation Receiver for  
 4 Ionospheric Sensing and Specification) is assimilated by some of the reanalyses.

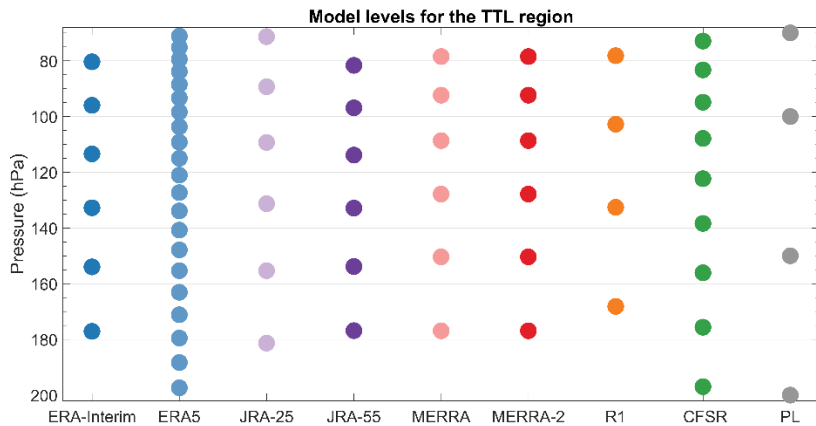


6 **Table 1.** List of GNSS-RO data assimilated by the reanalysis systems with starting dates prior to the end  
 7 of 2010.

8 Among the observational data sets, radiosonde and GNSS-RO data are our best source of  
 9 information about the TTL. While the reanalyses assimilate different versions of these data, it  
 10 is not automatic that they reproduce the data within their uncertainty *exactly*. For instance,  
 11 discrepancies exist between reanalysis stratospheric temperatures and those derived from their  
 12 radiance input data (Long et al., 2017). In fact, it is a subject of ongoing research how well  
 13 reanalyses fit the data they assimilate (Simmons et al., 2014, Wright and Hindley 2018). The  
 14 data assimilation systems combine information from a model, a set of observations and a priori  
 15 information weighted by their respective uncertainties. The degraded vertical resolution of the  
 16 reanalyses, compared to radiosonde and GNSS-RO data also leads to differences, especially for  
 17 derived quantities such as the tropopause location and temperature, which will be investigated  
 18 in the following evaluations.

19 The reanalysis models resolve the TTL with different vertical resolutions, as illustrated in **Fig.**  
 20 **1**. The number of model levels between 200 and 70 hPa varies among the reanalyses from a  
 21 low of 4 (NCEP-NCAR R1) to a high of 21 (ERA5), corresponding to vertical resolutions  
 22 between  $\sim 1.5$  km and  $\sim 0.2$  km. In addition to the native model levels, all reanalyses provide  
 23 post-processed data on standard pressure levels with at least four levels situated between 200  
 24 and 70 hPa (**Fig. 1**). The horizontal resolutions of the reanalysis products are approximately  
 25  $0.25^\circ \times 0.25^\circ$  (ERA5),  $0.7^\circ \times 0.7^\circ$  (ERA-Interim),  $0.63^\circ \times 0.5^\circ$  (MERRA-2),  $0.66^\circ \times 0.5^\circ$   
 26 (MERRA),  $0.56^\circ \times 0.56^\circ$  (JRA-55),  $1.13^\circ \times 1.13^\circ$  (JRA-25),  $0.5^\circ \times 0.5^\circ$  (CFSR), and  $1.9^\circ \times 1.9^\circ$   
 27 (R1).

1



2

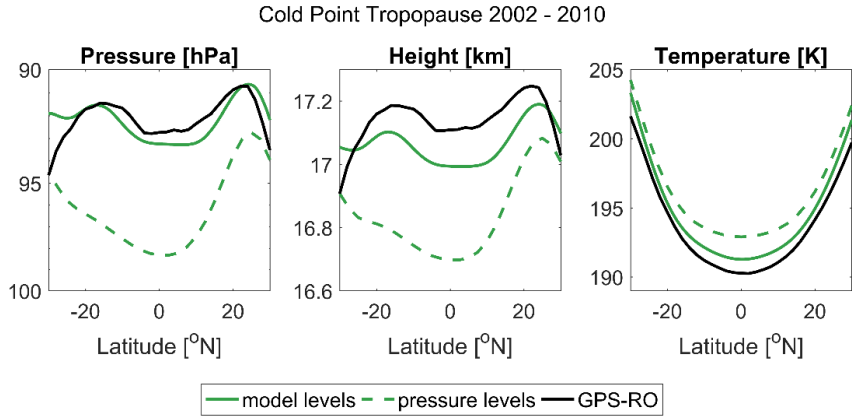
3 **Figure 1.** Model-level pressure values for different reanalysis data sets in the TTL using a fixed surface  
 4 pressure of 1013.25 hPa. Standard pressure levels (PL) in the TTL region are also shown.

5

### 6 2.3 Methods

7 Given the strong gradients of temperature and static stability in the TTL, the vertical resolution  
 8 of the reanalysis data sets is an important factor in cold point and lapse rate tropopause  
 9 calculations. For each reanalysis, tropopause heights and temperatures can be derived either  
 10 from model- or pressure-level data (**Fig 1**). A comparison of the CFSR cold point tropopause  
 11 based on model- and pressure-level temperature data is shown here to demonstrate the clear  
 12 advantage of the finer model-level resolution (**Fig. 2**). The cold point tropopause from CFSR  
 13 model-level data for the time period 2002–2010 agrees well with radio occultation results, with  
 14 differences of less than 1.5 K and 0.2 km at all latitudes. The tropopause derived from CFSR  
 15 pressure-level data, on the other hand, shows larger differences. This estimate is up to 0.4 km  
 16 too low and up to 3 K too warm, illustrating the need to use data with high vertical resolution  
 17 to identify and describe the tropopause. We derive the cold point and lapse rate tropopause  
 18 characteristics for each reanalysis using model-level data between 500 and 10 hPa at each grid  
 19 point at 6-hourly temporal resolution. Zonal and long-term averages are calculated by averaging  
 20 over all grid points, and represent the final step of data processing. For our calculations, the  
 21 cold point tropopause is defined as the coldest model level. The lapse rate tropopause is defined  
 22 as the lowest level at which the lapse rate decreases to  $2 \text{ K km}^{-1}$  or less, provided that the  
 23 average lapse rate between this level and all higher levels within 2 km does not exceed  $2 \text{ K km}^{-1}$   
 24 (World Meteorological Organization, 1957).

25



1

2 **Figure 2.** Latitudinal distributions of zonal-mean cold point tropopause pressure (left)  
 3 and altitude (centre) based on radio occultation data (black) and CFSR model-level (green solid) and  
 4 pressure-level (green dashed) data during 2002–2010.

5

6 The evaluation of the interannual variability (Section 4) is based on time series of  
 7 deseasonalized monthly temperature, pressure and altitude anomalies calculated relative to the  
 8 mean annual cycle during 2002–2010. To study variability driven by tropospheric and  
 9 stratospheric forcing, we identify and isolate the variations based on a standard multivariate  
 10 regression analysis:

$$11 T(t) = A_1 \cdot \text{QBO1}(t) + A_2 \cdot \text{QBO2}(t) + B \cdot \text{ENSO}(t) + D \cdot \text{VOL}(t). \quad (1)$$

12 Here  $\text{QBO1}(t)$  and  $\text{QBO2}(t)$  are orthogonal time series representing QBO variations constructed  
 13 as the first two EOFs of the Freie Universität Berlin (FUB) radiosonde stratospheric winds  
 14 (Naujokat, 1986).  $\text{ENSO}(t)$  is the multivariate ENSO index  
 15 (<https://www.esrl.noaa.gov/psd/enso/mei/>) and  $\text{VOL}(t)$  is the stratospheric aerosol optical depth  
 16 from the Global Space-based Stratospheric Aerosol Climatology (Thomason et al., 2018). The  
 17 standard error of the regression coefficients was derived based on the bootstrap method (Efron  
 18 and Tibshirani, 1993). The QBO temperature amplitude is calculated as the difference between  
 19 the averaged maxima and averaged minima values of the time series of the QBO temperature  
 20 variations  $A_1 \cdot \text{QBO1}(t) + A_2 \cdot \text{QBO2}(t)$ . For each QBO cycle of this time series, the absolute  
 21 temperature maximum and minimum are selected. In a second step, the means over all such  
 22 temperature maxima and minima are calculated to give the averaged maximum and minimum  
 23 values, respectively.

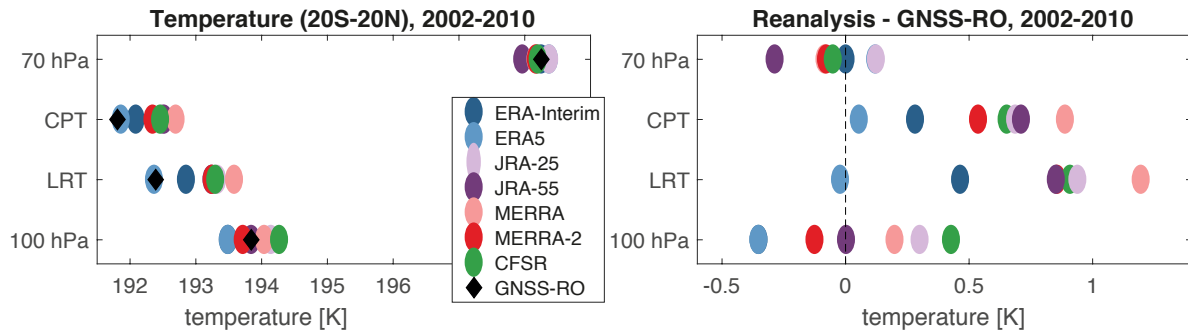
24

25 The long-term trends of the reanalyses temperature time series have been derived as the  
 26 regression coefficient of a linear function that provides the best fit in a least-squares sense. The  
 27 uncertainty in each long-term trend is calculated as the standard error of the slope with the  
 28 effective sample size adjusted to account for the corresponding lag-1 autocorrelation  
 29 coefficient. Significance is tested based on two-tailed test with a 95% confidence interval.

1 **3 Temperature and tropopause characteristics**

3 Tropical mean temperatures from reanalyses at two standard pressure levels (100 hPa and 70  
4 hPa) and at the two tropopause levels are compared to radio occultation data for the time period  
5 2002–2010 (**Fig. 3**). At 100 hPa, reanalysis temperatures agree well with radio occultation data  
6 with differences between  $-0.35$  K (too cold; ERA-Interim and ERA5) and  $0.43$  K (too warm;  
7 CFSR). At 70 hPa, the agreement is even better, with differences ranging from  $-0.29$  K (JRA-  
8 55) to  $0.12$  K (JRA-25). However, nearly all reanalyses show warm biases at both tropopause  
9 levels, with differences of up to  $1.2$  K compared to the observations. Most likely, the excess  
10 warmth of tropopause estimates based on reanalysis products stems from the limited vertical  
11 resolution of the reanalysis models in the TTL region. The best agreement is found for the  
12 reanalysis with the highest vertical resolution (ERA5;  $0.05$  K too warm at the cold point  
13 tropopause). The data set with the lowest vertical resolution (NCEP-NCAR R1) is  $2.2$  K too  
14 warm, outside the range displayed in Figure 3.

15



16  
17 **Figure 3.** Tropical mean ( $20^{\circ}\text{S}$ - $20^{\circ}\text{N}$ ) temperatures at 100 hPa, the lapse rate tropopause (LRT), the  
18 cold point tropopause (CPT) and 70 hPa from reanalyses and GNSS-RO data during 2002–2010 (left  
19 panel). Differences between the GNSS-RO and reanalysis temperatures are shown in the right panel. At  
20 100 hPa, ERA-Interim is hidden by ERA-5, at the LRT, MERRA-2 is hidden by JRA-55, and at 70 hPa,  
21 ERA5 is hidden by JRA-25 and MERRA is hidden by MERRA-2.

22 Temperature profile comparisons between 140 and 70 hPa at the native model levels ~~resolution~~  
23 have been conducted for the five most recent reanalyses (ERA5, ERA-Interim, JRA-55,  
24 MERRA-2, CFSR). All reanalyses tend to be colder than the observations in the tropical mean  
25 (**Fig. 4**), but differences are relatively small and the agreement is good overall. CFSR and ERA5  
26 agree best with the radio occultation data with mean biases of around  $-0.06$  K and  $-0.28$  K,  
27 respectively, averaged over the whole vertical range. ERA-Interim and MERRA-2 agree very  
28 well at upper levels but show large deviations on model levels near 100 hPa (ERA-Interim;  $-0.82$  K)  
29 and below 110 hPa (MERRA-2;  $-0.67$  K), respectively. The evaluation demonstrates  
30 that temperature comparisons at standard pressure levels (**Fig. 3**) can be biased by up to  $0.5$  K,  
31 with CFSR showing a positive bias ( $0.45$  K) at the 100 hPa standard pressure level but very  
32 good agreement ( $-0.05$  K) at nearby native model levels. Such biases can result from vertical  
33 interpolation of temperature data in regions with large lapse rate changes.

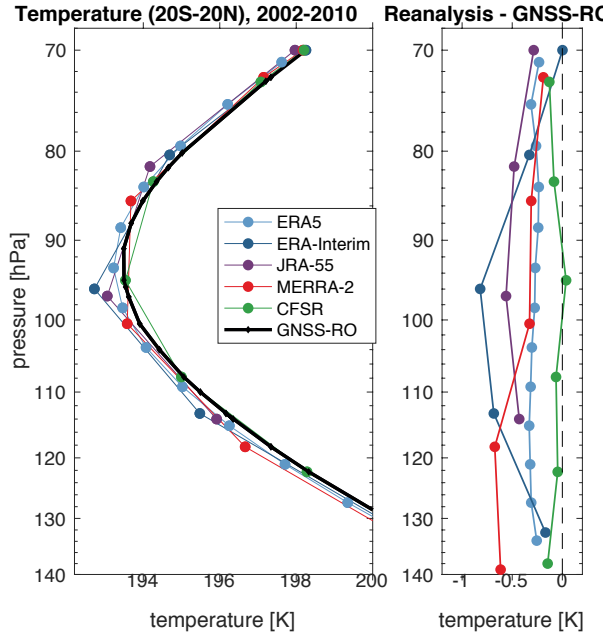


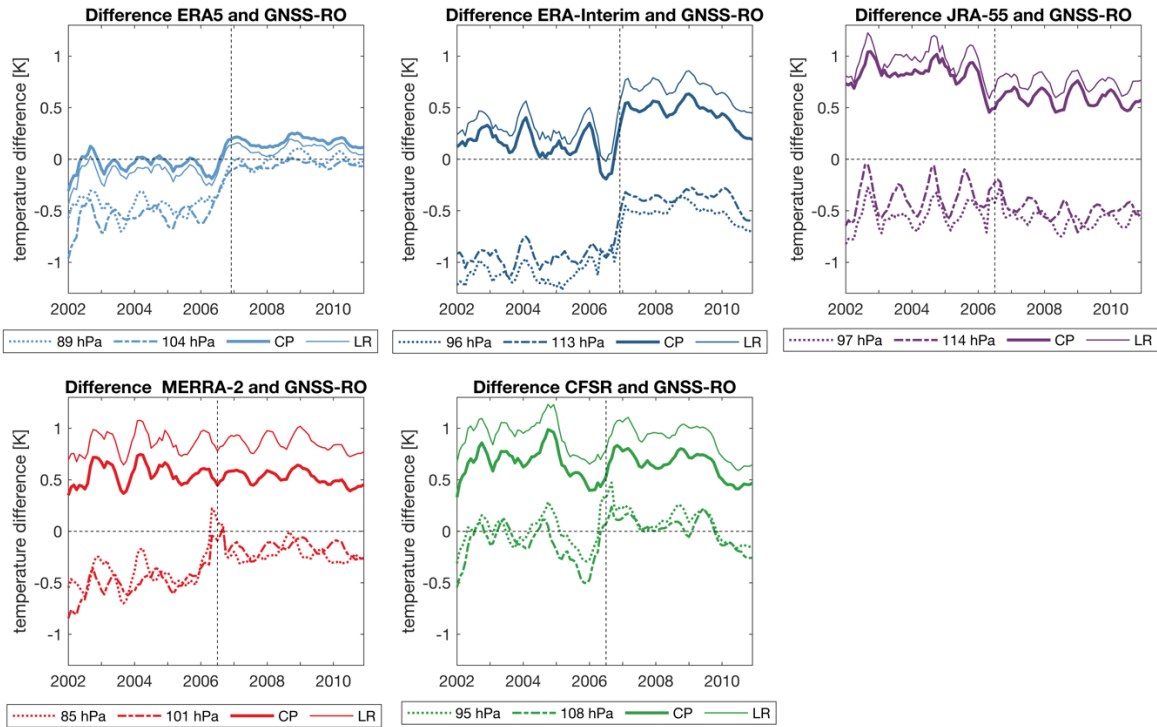
**Figure 4.** Tropical mean ( $20^{\circ}\text{S}$ – $20^{\circ}\text{N}$ ) temperature profiles at reanalysis model levels between 140 and 70 hPa (left panel) during 2002–2010 and differences between reanalysis and GNSS-RO temperatures (right panel).

Comparing the temperature profiles to the tropopause values (Fig. 3 and 4) reveals that despite the five reanalyses having negative biases at model levels, they mostly have positive biases at the cold point and lapse rate tropopause levels. As the discrete values corresponding to reanalysis model levels are unable to reproduce the true minimum temperature as recorded in a near-continuous profile, this difference is expected for the cold point tropopause. Similarly, the lapse rate tropopause criteria might typically be fulfilled at lower levels for data at coarser resolution, thus resulting in a warm bias at the lapse rate tropopause on average. Overall, our results indicate that the negative temperature bias at model levels is more than cancelled out by the positive bias introduced when calculating the cold point and lapse rate tropopauses. Linking the temperature profile and tropopause comparisons, this ‘bias shift’ is about 0.3 K for ERA5, 0.6 K for CFSR and 1 K or larger for ERA-Interim, MERRA-2 and JRA-55. In consequence, ERA5, with both a small negative bias at the model levels and a small bias shift provides the most realistic tropopause temperatures. CFSR also has a relatively small bias shift, but the relatively unbiased temperature profile does not permit any error cancelation via this shift, so that cold point and lapse rate tropopause levels based on CFSR are systematically too warm.

Agreement between the reanalysis temperature profiles and GNSS-RO data clearly improves when the comparison is restricted to the 2007–2010 time period, when the more densely-sampled COSMIC data were assimilated (Table 1). This point is illustrated by comparison of temperature time series from reanalyses and observations at two model and both tropopause levels (Fig. 5). For ERA5, ERA-Interim and MERRA-2, the cold bias with respect to GNSS-RO at model levels decreases after 2007, most likely because of the high number of daily COSMIC profiles available for assimilation from this time onwards. Cold biases at model levels are accompanied by warm biases in the tropopause temperatures, which, for ERA-Interim and ERA5, increase after 2007. As the increase at all levels is very similar, this indicates that the

1 advantage of a reduced temperature bias at model levels comes at the expense of an increased  
 2 temperature bias at the tropopause. CFSR and MERRA-2 show no such systematic change of  
 3 their tropopause temperatures over time when compared to GNSS-RO data. JRA-55 is the only  
 4 reanalysis product for which cold point and lapse rate tropopause temperatures agree slightly  
 5 better with GNSS-RO estimates after 2007.

6



7

8 **Figure 5.** Tropical mean ( $20^{\circ}\text{S}$ - $20^{\circ}\text{N}$ ) time series of temperature differences between reanalysis and  
 9 radio occultation at the cold point (CP) and lapse rate (LR) tropopause levels, as well as selected  
 10 reanalysis model levels. Vertical lines indicate when the assimilation of COSMIC radio occultation data  
 11 started.

12

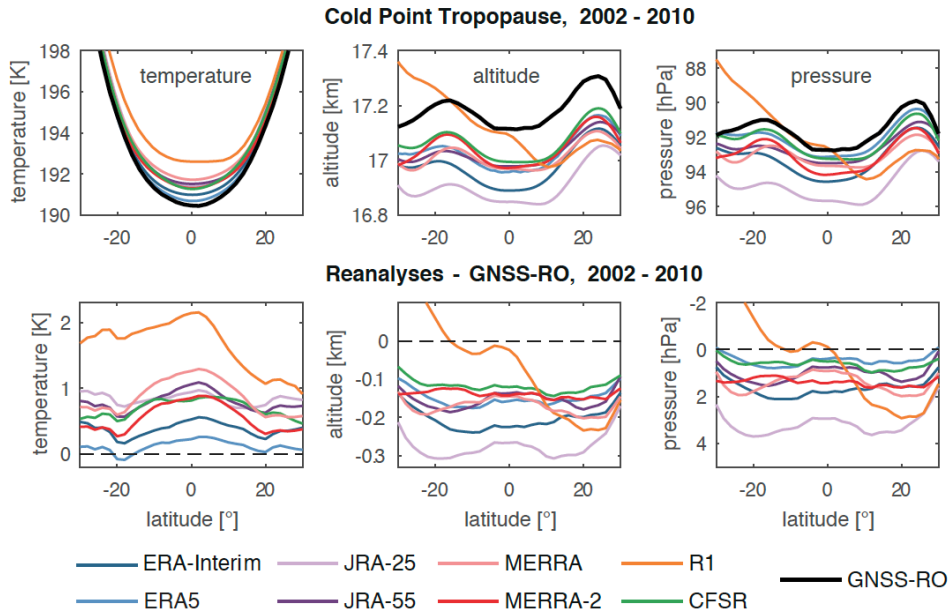
13 Evaluations of the latitudinal structure of the cold point tropopause for 2002–2010 are based on  
 14 comparisons to radio occultation data (**Fig. 6**). All reanalysis data sets produce tropopause  
 15 levels that are too low and too warm, with the latter related to vertical resolution as explained  
 16 above. The observations show that average cold point temperatures are lowest right around the  
 17 equator. The reanalyses fail to reproduce this latitudinal gradient, indicating more constant cold  
 18 point temperatures across the inner tropics between  $10^{\circ}\text{S}$  and  $10^{\circ}\text{N}$  with a less pronounced  
 19 minimum at the equator. As a consequence, the largest differences in cold point tropopause  
 20 temperatures relative to GNSS-RO data are at the equator and the best agreement is around  
 21  $20^{\circ}\text{S}$ / $20^{\circ}\text{N}$  for all reanalysis data sets.

22

23

1 The cold point altitude and pressure exhibit little north–south variability, ranging from 16.9 km  
 2 (94 hPa) to 17.2 km (91.8 hPa). With respect to the seasonal cycle, it is well known that the  
 3 temperature and altitude of the cold point tropopause are linked, with the coldest temperatures  
 4 and highest altitudes observed during boreal winter (e.g., Seidel et al., 2001; Kim and Son,  
 5 2012). This relationship does not hold in the meridional direction: the highest cold point  
 6 altitudes are located around 20°S/20°N, while the lowest cold point temperatures are located  
 7 near the equator. The higher altitude/lower pressure of the cold point tropopause around  
 8 20°S/20°N results from zonally-variable features linked to tropospheric pressure regimes, such  
 9 as particularly low tropopause pressures over the Tibetan plateau during boreal summer (Kim  
 10 and Son, 2012). The reanalysis data sets capture most of this latitudinal structure, showing  
 11 roughly constant differences between about 0.1 and 0.2 km (0–2 hPa). The largest differences  
 12 are found for NCEP-NCAR R1 in the Southern Hemisphere, where the cold point tropopause  
 13 based on R1 is both higher and warmer than observed. The best agreement with respect to cold  
 14 point temperatures is found for ERA5 and ERA-Interim, which are around 0.2 K and 0.4 K  
 15 warmer than the radio occultation data, respectively. All other reanalysis data sets are in close  
 16 agreement with each other, with differences from the observations of between 0.5 K and 1 K.  
 17 The altitude and pressure of the cold point tropopause are captured best by ERA5, CFSR,  
 18 MERRA, MERRA-2 and JRA-55, which all produce cold point tropopauses that are slightly  
 19 too low (~0.1 km). ERA-Interim, despite very good agreement in cold point temperature, shows  
 20 slightly larger biases in cold point altitude (~0.2 km) relative to the GNSS-RO benchmark.  
 21 Zonal mean cold point tropopause temperatures, altitudes and pressures during 1981–1990 and  
 22 1991–2002 are shown for all reanalyses in the supplementary Figure S1.

23

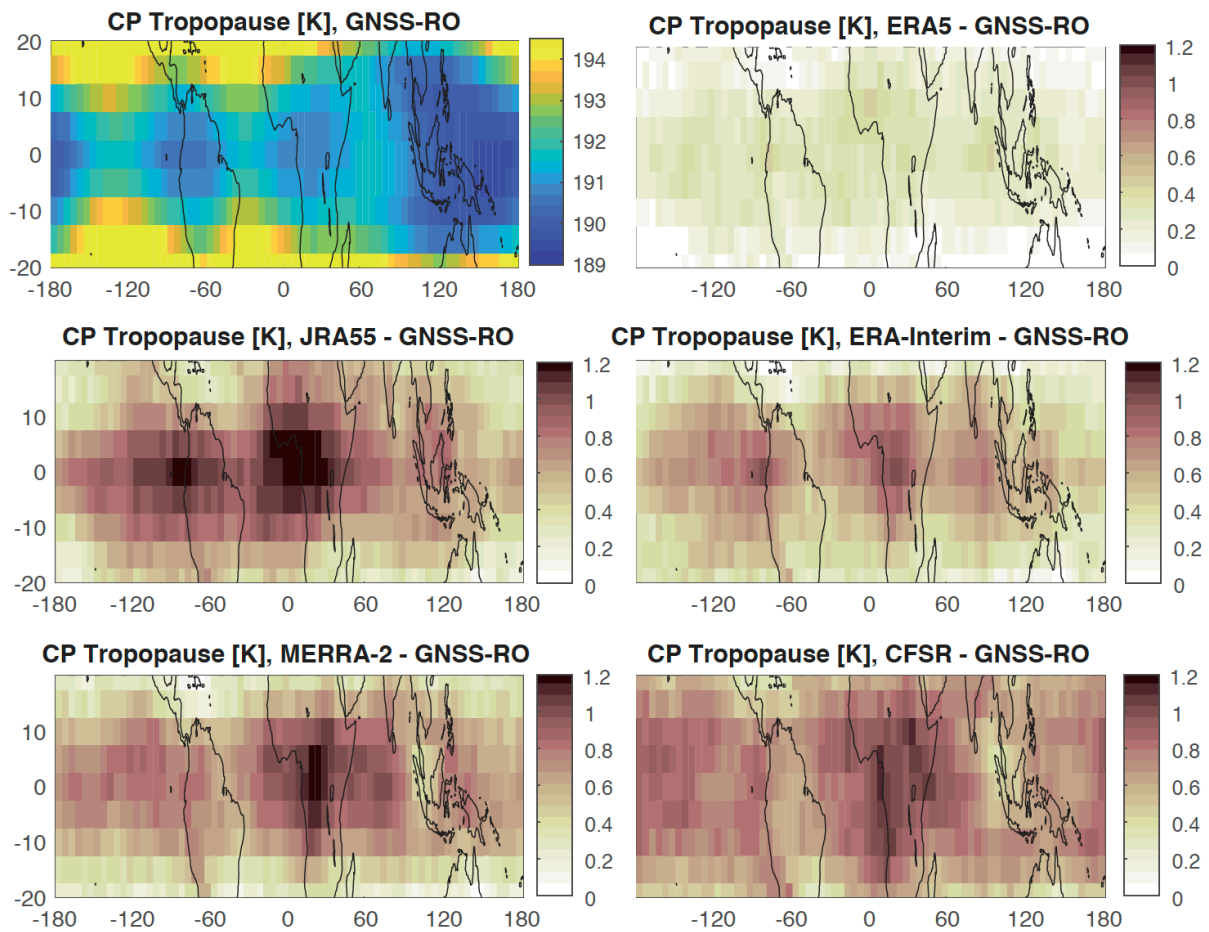


24

25 **Figure 6.** Latitudinal distributions of zonal-mean cold point tropopause temperature (left), altitude  
 26 (centre) and pressure (right) based on radio occultation data and reanalysis products during 2002–2010  
 27 (upper row). Differences between radio occultation and reanalysis estimates are shown in the lower row.

1 We investigate the temperature biases and their maxima near the equator by analysing latitude–  
 2 longitude variations in the cold point tropopause relative to GNSS-RO estimates for four of the  
 3 reanalyses (Fig. 7). To show differences at relatively high spatial resolution, we focus on the  
 4 period 2007–2010. A wealth of observational studies has shown that the coldest tropopause  
 5 temperatures are located over the “maritime continent” (i.e. the general area of Indonesia)  
 6 and the West Pacific (Highwood and Hoskins, 1998), with secondary minima over equatorial  
 7 South America and Africa coinciding with other centres of deep convective activity (Gettelman  
 8 et al., 2002). The colocation of tropospheric convective activity with zonal asymmetries in cold  
 9 point temperature can be explained by the radiative cooling effects of cirrus clouds overlying  
 10 deep convection (Hartmann et al., 2001) or diabatic cooling associated with convective  
 11 detrainment (Sherwood et al., 2003). Furthermore, it has been suggested that the response of  
 12 equatorial waves to convective heating influences the structure of the cold point tropopause  
 13 (Kim and Son, 2012; Nishimoto and Shiotani, 2012; Nishimoto and Shiotani, 2013). The  
 14 dominant wave modes responsible for cold point temperature variability are linked to equatorial  
 15 Kelvin waves and the Madden-Julian oscillation.

16



17

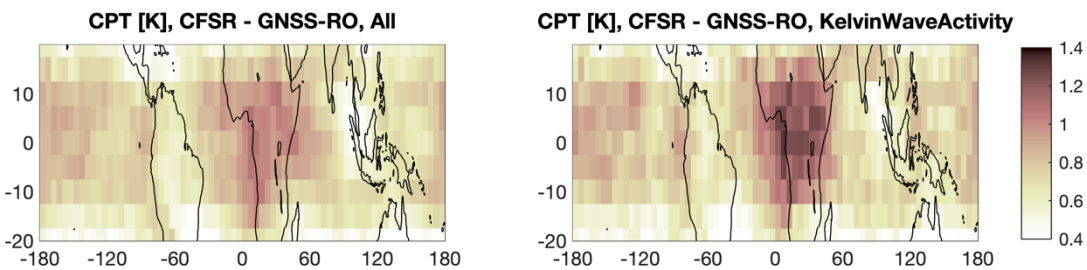
18 **Figure 7.** Latitude–longitude distributions of annual mean GNSS-RO cold point temperatures (upper  
 19 and differences between cold point temperatures from individual reanalyses and those from GNSS-  
 20 RO during 2007–2010 (lower panels).

21

1 For the analysed reanalyses (ERA5, ERA-Interim, MERRA-2, JRA55, and CFSR), differences  
2 with respect to the observations are largest in the inner tropics over central Africa, reaching  
3 values 50% to 100% greater than the zonal mean differences. This region is characterized by a  
4 local cold point minimum that results from deep convection and its interaction with equatorial  
5 waves. There is also evidence of a secondary maximum in the differences over equatorial South  
6 America or the East Pacific, although the magnitude and location of this maximum differ among  
7 the reanalyses.

8 The convective centre over the Western Pacific warm pool, where the cold point tropopause is  
9 coldest, does not show enhanced biases relative to the observations. One possible explanation  
10 for the bias distribution might link the enhanced temperature differences to Kelvin wave activity  
11 that maximizes over Central Africa but is weaker over the West Pacific (Kim et al., 2019). As  
12 the Kelvin waves disturb the temperature profile at small vertical scales, the reanalyses may be  
13 particularly unsuited to estimate cold point temperatures in regions of strong Kelvin wave  
14 activity. We average cold point temperatures from reanalyses and observations over time  
15 periods of enhanced Kelvin wave activity. For CFSR, composite differences for periods with  
16 enhanced wave activity are compared in **Fig. 8** to mean differences averaged over the whole  
17 2007–2010 period. While mean biases over Central Africa are less than 1 K, average differences  
18 during periods of enhanced Kelvin wave activity are as large as 1.4 K. The same is true for  
19 other reanalyses (not shown here), with the exception of ERA-Interim, suggesting that in most  
20 cases Kelvin waves contribute to the spatial structure of biases in cold point tropopause  
21 estimates based on reanalysis products.

22



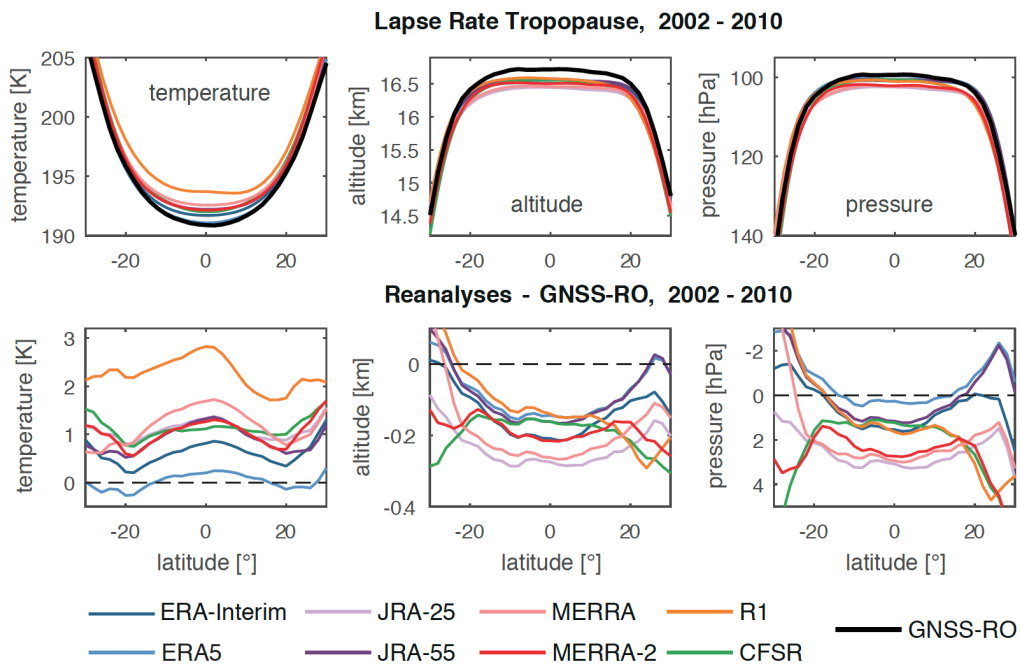
23  
24 **Figure 8.** Latitudinal-longitude sections of the differences between GNSS-RO and CFSR cold point  
25 temperatures for 2007-2010 (left panel) and for time periods of high wave activity (right panel).

26

27 The zonal mean lapse rate tropopause (**Fig. 9**) at the equator is found at similar temperatures  
28 and heights as the cold point tropopause, being only slightly warmer and lower. Poleward of  
29 10°S/10°N, however, the lapse rate tropopause height decreases considerably faster than the  
30 cold point height, since the cold point is more often located at the top of the inversion layer  
31 while the lapse rate tropopause is located at the bottom of the inversion layer (Seidel et al.,  
32 2001). Lapse rate tropopause temperatures based on reanalysis data are on average about 0.2 K  
33 to 1.5 K too warm when compared to radio occultation data (see **Fig. 3** and associated  
34 discussion) with best agreement for ERA5 and ERA-Interim. Consistent with this temperature  
35 bias, lapse rate tropopause levels based on reanalysis data are about 0.2 km to 0.4 km lower

1 than those based on radio occultation data. The latitudinal structure of lapse rate tropopause  
 2 temperatures reveals slightly larger biases at the equator and better agreement between  $10^{\circ}$ – $20^{\circ}$   
 3 in each hemisphere, and is generally very similar to the latitudinal distribution of biases in cold  
 4 point temperatures (Fig. 6). The altitude of the lapse rate tropopause shows considerable **zonal**  
 5 meridional variability, ranging from 14.5 km to 16.7 km. All reanalyses capture the plateau in  
 6 lapse rate tropopause altitudes between  $20^{\circ}$ S and  $20^{\circ}$ N and the steep gradients in these altitudes  
 7 on the poleward edges of the tropics. Zonal mean lapse rate tropopause temperatures, altitudes  
 8 and pressures during 1981-1990 and 1991-2002 are shown for all reanalyses in the  
 9 supplementary Figure S2.

10



11

12 **Figure 9.** Latitudinal distributions of zonal-mean lapse rate tropopause temperature (left)  
 13 (centre) and pressure (right) based on radio occultation data and reanalysis products during 2002–2010  
 14 (upper row). Differences between radio occultation and reanalysis estimates are shown in the lower row.

15

16

17

1 **4 Interannual variability and long-term changes**

2

3 It has long been recognized that inter-annual variations in TTL temperatures are strongly  
4 affected by both tropospheric (e.g. ENSO) and stratospheric (e.g. QBO, solar, volcanic)  
5 variability (Randel et al., 2000; Zhou et al., 2001, Krüger et al 2008). Time series of  
6 deseasonalized monthly 70 hPa temperature anomalies and cold point temperature, pressure  
7 and altitude anomalies are shown in **Fig. 10**. Anomalies are calculated relative to the mean  
8 annual cycle during 2002–2010 for each dataset. The interannual variability of ERA5 is not  
9 analysed due to the short data record available at the time of the analysis. The performance of  
10 the reanalyses with respect to both the spread among reanalyses and their agreement with  
11 observations is much better at the 70 hPa level than at the cold point level. The older reanalyses  
12 NCEP-NCAR R1 and JRA-25 generally show larger deviations from the RAOBCORE time  
13 series. The level of agreement among the reanalyses and between reanalyses and observations  
14 improves over time, with a step-like improvement around 1998–1999 that is likely associated  
15 with the TOVS-to-ATOVS transition. The higher vertical resolution of measurements from the  
16 ATOVS suite (see, e.g. Figure 7 in Fujiwara et al., 2017) is known to reduce differences among  
17 the reanalysis with respect to stratospheric temperature (Long et al., 2017) and polar diagnostics  
18 (Lawrence et al., 2018). Within the TTL, temperature biases decrease from values of 1–2 K to  
19 around 0.5 K following the TOVS-to-ATOVS transition. This agreement improves further after  
20 2002, when many of the more recent reanalyses started assimilating AIRS and GNSS-RO data  
21 (**Table 1**; see also Figure 8 in Fujiwara et al., 2017).

22

23 Interannual variability at 70 hPa is dominated by the stratospheric QBO signal, which is  
24 reproduced by all reanalysis data sets. The amplitudes of the QBO temperature variations in all  
25 datasets based on a multilinear regression analyses over 1981-2010 are shown in **Fig. 11**. At 70  
26 hPa, the observational radiosonde data sets give QBO variations of 2.1–2.2 K. Reanalyses agree  
27 well with the observations and show QBO variations of 2–2.4 K. The only exception is NCEP-  
28 NCAR R1, which clearly underestimates the signal compared to radiosondes and other  
29 reanalyses, with an amplitude of 1.7 K. Best agreement with the radiosonde data sets is found  
30 for MERRA-2, MERRA and CFSR. The influence of ENSO on TTL temperatures (not shown  
31 here) shows large longitudinal variations with positive anomalies over the maritime continent  
32 and West Pacific and negative anomalies over the East Pacific. While the zonally resolved  
33 response patterns agree well between observations and reanalyses, the zonal mean responses  
34 are not significant. Positive temperature anomalies following the eruptions of El Chichón in  
35 1982 can be detected in Fig. 10 for all reanalyses, consistent with the results of Fujiwara et al.  
36 (2015). Following the Mount Pinatubo eruption in 1991, small positive temperature anomalies  
37 are evident at the 70 hPa level around the beginning of 1992. However, no positive temperature  
38 anomalies are found at the cold point during this time (see Fujiwara et al., 2015 for a more  
39 detailed analysis).

40

41

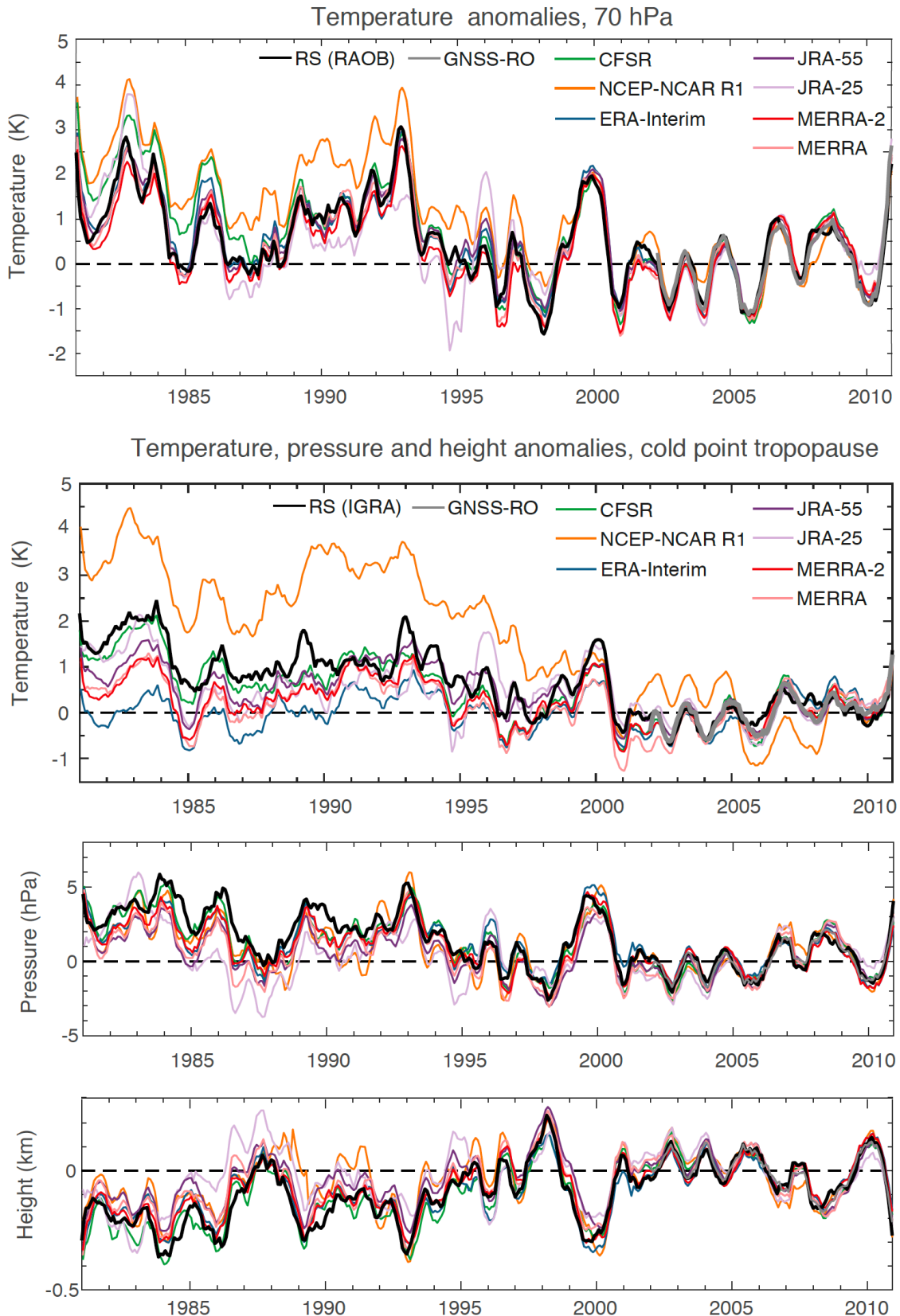
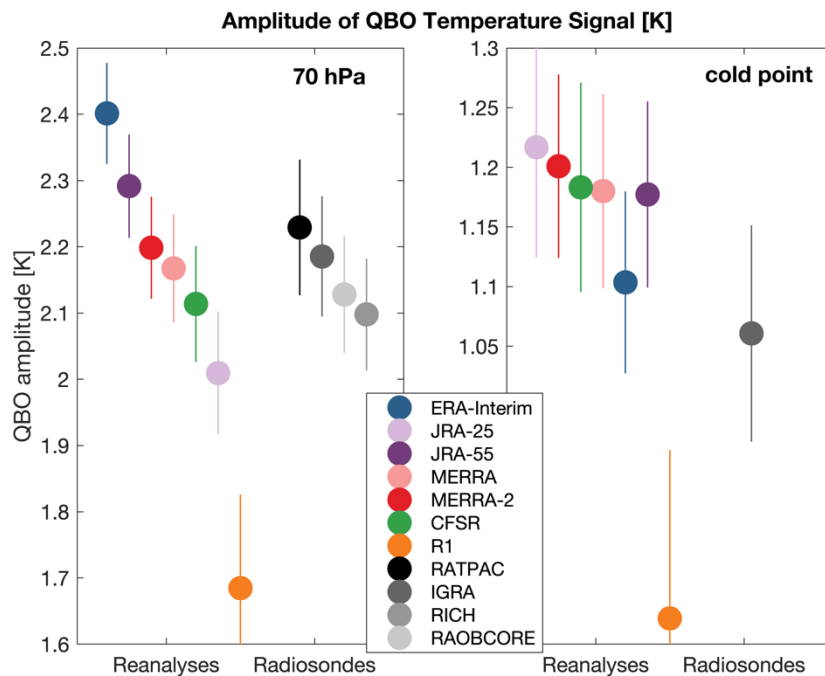


Figure 10. Time series of deseasonalized anomalies in 70 hPa temperature (upper), cold point temperature (upper middle), cold point pressure (lower middle) and cold point altitude (lower) averaged over the tropics ( $20^{\circ}\text{S}$ – $20^{\circ}\text{N}$ ) and evaluated relative to the reference period 2002–2010. Time series are shown for reanalysis products, radiosonde data (RAOB and IGRA) and radio occultation data (GNSS-RO). Time series are smoothed with a 7-months running mean.

1 At the cold point, NCEP-NCAR R1 is a clear outlier, with much warmer temperature anomalies  
 2 than any other data set during the period prior to 2005 (Fig. 10). However, differences among  
 3 the more recent reanalyses are also relatively large, with ERA-Interim (on the lower side) and  
 4 CFSR (on the upper side) showing differences as large as 2 K in the early years of the  
 5 comparison. Given that existing homogenized radiosonde data sets also show deviations of up  
 6 to 1.5 K at this level (Figure 2 in Wang et al., 2012), we cannot deduce which reanalysis data  
 7 set is most realistic. Note that the radiosonde time series from IGRA shown here should not be  
 8 used for evaluating long-term changes (see Wang et al., 2012 for details), but only for assessing  
 9 the representation of interannual variability. Periods of particularly pronounced interannual  
 10 variability alternate with relatively quiescent ones. The amplitude of interannual variability  
 11 (Fig. 10) and the QBO temperature signal (Fig. 11) are weaker at the cold point than at 70 hPa,  
 12 but are still well captured by all of the reanalysis data sets except for NCEP-NCAR R1.  
 13

14 Interannual variability in cold point pressure and altitude (Fig. 10) shows better agreement  
 15 among the data sets than that in cold point or 70 hPa temperature. During the first 15 years of  
 16 the record, the reanalysis cold point tropopause levels are mostly shifted toward ~~higher~~ lower  
 17 altitudes and higher pressures, consistent with higher temperatures during this period.  
 18 Anomalies in cold point temperature are in most cases matched by anomalies in cold point  
 19 pressure and altitude, with a warmer cold-point temperature (e.g. around 1999–2000) corresponding to lower tropopause (negative altitude anomaly and positive pressure anomaly)  
 20 and vice versa. The older reanalyses NCEP-NCAR R1 and JRA-25 again show the largest  
 21 overall differences. The agreement improves over time, with the most consistent results found  
 22 for the period after 2002.  
 23

24  
 25

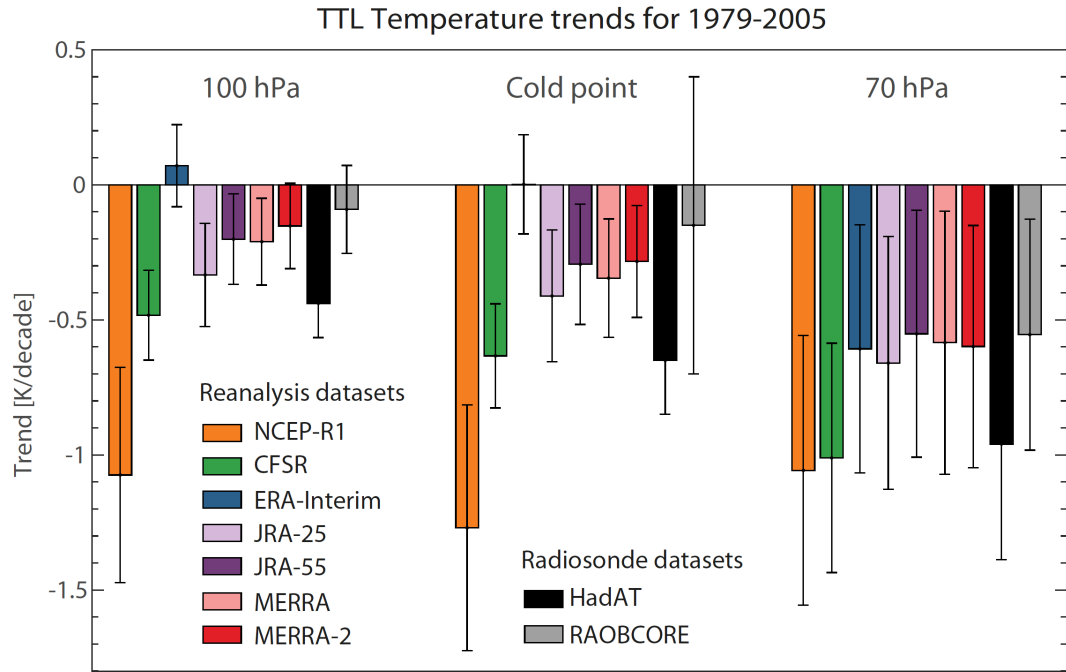


26  
 27 **Figure 11.** Amplitude of QBO temperature signal for 10°S-10°N at 70 hPa and the cold point derived  
 28 from a multilinear regression analyses for radiosonde and reanalysis data sets for the period 1981-2010.

1 Long-term temperature changes are evaluated over the 1979–2005 time period due to the  
2 availability of adjusted tropopause trends from radiosonde data sets (see Wang et al., 2012 for  
3 details). Both radiosonde records suggest significant cooling at the 70 hPa level (**Fig. 12**).  
4 Trends derived from reanalysis data can be problematic due to changes in the assimilated  
5 observations. Given this potential limitation, it is of interest to examine whether the reanalysis  
6 trends are consistent with the hypothetically more reliable trends derived from homogenized  
7 observational records. At 70 hPa, temperature trends based on the reanalysis data sets span  
8 almost exactly the same range (−0.5 to −1.1 K/decade) as those based on the radiosonde data  
9 sets (−0.5 to −1 K/decade). All reanalysis- and observationally-based trends are significant at  
10 this level, confirming the stratospheric cooling reported by many previous studies (e.g., Randel  
11 et al., 2009). Satellite data from the Microwave Sounding Unit channel 4 (~13–22 km) suggests  
12 smaller trends of around −0.25 K/decade over 1979–2005 (Maycock et al., 2018) or −0.4  
13 K/decade over 1979–2009 (Emanuel et al., 2013). However, the much broader altitude range  
14 of this MSU channel includes both stratospheric and tropospheric levels, which impedes a direct  
15 comparison with trends at 70 hPa.

16 At the 100 hPa and cold point levels, the situation is completely different. The available  
17 adjusted radiosonde data sets show in some cases uncertainties larger than the respective  
18 temperature trends at these levels. Only a few of the available data sets indicate a statistically  
19 significant cooling based on a methodology that adjusts the cold point trend to account for  
20 nearby fixed pressure-level data and day–night differences (Wang et al., 2012). Based on the  
21 trends shown in Wang et al. (2012) for five adjusted radiosonde data sets, we show here the  
22 smallest and largest reported trends and consider their range (including the reported error bars)  
23 as the observational uncertainty range. Similar to the observations, the reanalysis data sets  
24 suggest a large range in cold point temperature trends, from no trend at all (0 K/decade for  
25 ERA-Interim) to a strong cooling of −1.3 K/decade (NCEP-NCAR R1). The latter is outside of  
26 the observational uncertainty range and can thus be considered unrealistic. All other reanalyses  
27 suggest small but significant cooling trends of −0.3 K/decade to −0.6 K/decade. JRA-25, JRA-  
28 55, MERRA, and MERRA-2 agree particularly well and produce trends in the middle of the  
29 observational uncertainty range. Overall, due to the large uncertainties in radiosonde-derived  
30 cold point temperature trends, all reanalyses except for R1 are statistically consistent with at  
31 least one of the observational data sets.

32



1

2 **Figure 12.** Linear trends in tropical mean (20°S–20°N) temperature (K/decade) at 100 hPa, the cold  
 3 point and 70 hPa for the time period 1979-2005. Error bars indicate  $\pm 2\sigma$  uncertainty in the trend and  
 4 account for serial auto-correlation.

5 Temperature trends at 100 hPa are very similar to trends at the cold point level, and again  
 6 suggest consistency among most of the reanalysis and radiosonde data sets, with the notable  
 7 exception of R1. Nearly all data sets suggest slightly smaller cooling trends ( $-0.15$  K/decade to  
 8  $-0.5$  K/decade) relative to the cold point consistent with the fact that the cold point is at slightly  
 9 higher altitudes than 100 hPa. Among the data sets, only ERA-Interim produces a warming  
 10 trend (0.07 K/decade), although this result is not statistically significant.

11

## 12 5 Summary

13 Meteorological reanalyses are widely used in scientific studies of TTL processes being utilized  
 14 as “stand in observations” or for driving transport models. The most recent atmospheric  
 15 reanalysis data sets (ERA5, ERA-Interim, MERRA-2, JRA-55, and CFSR) all provide realistic  
 16 representations of the major characteristics of temperature structure within the TTL for 2002-  
 17 2010. There is good agreement between reanalysis estimates of tropical mean temperatures  
 18 between 140 and 70 hPa and GNSS-RO retrievals, with relatively small cold biases for most  
 19 data sets. CFSR shows the best agreement with GNSS-RO in this layer with a mean bias of  
 20  $-0.06$  K. Agreement between the temperature profiles and the GNSS-RO data clearly improves  
 21 when the comparison is restricted to the period after 2007, when the densely-sampled COSMIC  
 22 data were assimilated by all reanalyses.

23 Temperatures at the cold point and lapse rate tropopause levels show warm biases in reanalyses  
 24 when compared to observations. This tropopause-level warm bias is opposite to the cold bias  
 25 found at all model levels and is most likely related to difficulties in determining the true cold

1 point and lapse rate tropopause levels from discrete temperature profiles with coarse vertical  
2 resolution. Our analysis confirms that the magnitude of the bias shift is consistent with the  
3 vertical resolution of the reanalysis data, with the smallest bias shifts found for data sets with  
4 the highest vertical resolution around the tropopause (ERA5 and CFSR). The negative  
5 temperature bias at model levels is often cancelled out by the positive bias introduced when  
6 identifying the lapse rate and cold point tropopause locations. As a result, ERA5, which has a  
7 small negative bias at model levels and a small bias shift, has the most realistic tropopause  
8 temperatures, while CFSR, which produces the most realistic model-level temperature profile,  
9 has a warm bias of 0.6–0.9 K at the cold point and lapse rate tropopause levels. Older reanalyses  
10 like MERRA, JRA-25 and especially NCEP-NCAR R1 show the largest temperature biases at  
11 the tropopause levels.

12 The zonal structure of tropopause temperature reveals that the biases in reanalysis relative to  
13 observations maximise at or near the equator. All of the recent reanalyses produce a realistic  
14 horizontal structure of cold point temperature with minima corresponding to the centres of  
15 tropical deep convection. Differences between reanalyses and observations are greatest over  
16 equatorial Africa. These enhanced differences are possibly related to Kelvin wave activity and  
17 associated disturbances in TTL temperatures that also maximize in this region. Further  
18 investigation of seasonal variability in the cold point tropopause, including detailed analysis of  
19 this feature, will be conducted in a follow-up study.

20 Interannual variability in reanalysis temperatures is best constrained in the upper TTL (70 hPa),  
21 with larger differences at lower levels such as the cold point and 100 hPa. The reanalyses  
22 reproduce the temperature responses to major dynamical and radiative signals such as volcanic  
23 eruptions and the QBO. Agreement among the reanalyses and between the reanalyses and  
24 observations generally improves over time, with a step-like improvement around the TOVS-to-  
25 ATOVS transition in 1998–1999 and in 2006 with the beginning of assimilation of COSMIC  
26 GNSS-RO data. Interannual variability is lower at the cold point and 100 hPa relative to 70  
27 hPa, but with larger month-to-month fluctuations causing larger discrepancies among the  
28 reanalyses. As at 70 hPa, NCEP-NCAR R1 is a clear outlier. Interannual variability in cold  
29 point pressure and altitude shows better agreement than that in TTL temperature. Anomalies in  
30 cold point temperatures are in most cases matched by corresponding anomalies in cold point  
31 pressure and altitude.

32 Long-term reanalysis trends in temperature at 70 hPa show good agreement with trends derived  
33 from adjusted radiosonde data sets. All reanalyses and observational data sets indicate  
34 significant stratospheric cooling at this level of around  $-0.5$  K/decade to  $-1$  K/decade. At the  
35 100 hPa and cold point levels, both adjusted radiosonde data sets and reanalyses indicate large  
36 uncertainties in temperature trends. Reanalysis-based estimates at the cold point range from no  
37 trend at all (0 K/decade for ERA-Interim) to strong cooling of  $-1.3$  K/decade (NCEP-NCAR  
38 R1). While the latter is outside of the observational uncertainty range and can be considered  
39 unrealistic, all other reanalyses data sets agree with at least one of the observational data sets  
40 within uncertainties. The bulk of the reanalyses are in good agreement at these levels,  
41 suggesting small but significant cooling trends of  $-0.3$  K/decade to  $-0.6$  K/decade that are  
42 statistically consistent with trends based on the adjusted radiosonde data sets.

1 Advances of the reanalysis and observational systems over the last decades have led to a clear  
2 improvement of the TTL reanalyses products over time. In particular, the more recent  
3 reanalyses ERA-Interim, ERA5, MERRA-2, CFSR and JRA-55 mostly show very good  
4 agreement after 2002 in terms of the vertical TTL temperature profile, meridional tropopause  
5 structure and interannual variability. Temperatures at the cold point and lapse rate, on the other  
6 hand, are too high for most reanalyses, regardless of production date. As these differences  
7 maximise over Central Africa, a centre of deep convective activity, chemistry-transport models  
8 driven by reanalyses and simulating air mass transport into the stratosphere, can be expected to  
9 have too little dehydrations and too high water vapor. Furthermore, all reanalyses place the cold  
10 point tropopause too low in altitude relative to observations. This displacement can have  
11 important implications for studies that compare water vapor and ice observations with the  
12 position of the cold point tropopause derived from reanalyses data, as enhanced ice and water  
13 vapour contents could be erroneously attributed to deep convection crossing the tropopause.

14 Depending on the particular application, different reanalyses offer different advantages such as  
15 a realistic cold point temperature (e.g., ERA5), small bias in the TTL temperature profile (e.g.,  
16 CFSR), realistic spatial distribution of the cold point temperature (e.g., ERA-Interim),  
17 continuous TTL temperature time series through 2006 (e.g., JRA55), or a realistic  
18 representation of signals of interannual variability (e.g., MERRA-2). Their use in model  
19 simulations and in comparisons with climate model output should be tailored to their specific  
20 strengths and weaknesses.

21 **Author contributions.** ST developed the idea for this paper and carried out the evaluations  
22 with contributions from all co-authors. SD and BL provided the reanalyses tropopause and  
23 profile data. RPK provided the GNSS-RO tropopause, wave activity and temperature profile  
24 data. J. S. Wang provided the radiosonde tropopause data. ST wrote the manuscript with  
25 contributions from all co-authors.

26 **Data availability.** Reanalyses, GNSS-RO and radiosonde data can be inquired about by  
27 contacting the authors

28 **Competing interests.** The authors declare that they have no conflict of interest.

29 **Acknowledgements.** We thank the reanalysis centres for providing their support and data  
30 products. We thank C. Bloecker from the Global Modeling and Assimilation Office, NASA  
31 Goddard Space Flight Center for providing information on the GNSS-RO data assimilated in  
32 MERRA-2. ERA5 data were generated using Copernicus Climate Change Service Information.  
33 MERRA-2 data access was through the Global Modeling and Assimilation Office (GMAO,  
34 2015). The work of S. Tegtmeier was funded by the Deutsche Forschungsgemeinschaft (DFG,  
35 German Research Foundation) – TE 1134/1. Contributions from J.S. Wright were supported by  
36 the National Natural Science Foundation of China (20171352419) via a joint DFG–NSFC  
37 funding initiative.

1    **References**

2    Anthes, R. A., Bernhardt, P. A., Chen, Y., Cucurull, L., Dymond, K. F., Ector, D., Healy, S. B., Ho, S.-  
3    P., Hunt, D. C., Kuo, Y.-H., Liu, H., Manning, K., McCormick, C., Meehan, T. K., Randel, W. J.,  
4    Rocken, C., Schreiner, W. S., Sokolovskiy, S. V., Syndergaard, S., Thompson, D. C., Trenberth, K. E.,  
5    Wee, T.-K., Yen, N. L., and Zeng, Z.: The COSMIC/FORMOSAT-3 Mission: Early Results, *Bulletin*  
6    of the American Meteorological Society

7    89, 313, <https://doi.org/10.1175/BAMS-89-3-313>, 2008.

7    Beyerle, G., Schmidt, T., Michalak, G., Heise, S., Wickert, J., and Reigber, C.: GPS radio occultation  
8    with GRACE: Atmospheric profiling utilizing the zero difference technique, *Geophysical Research*  
9    Letters

32, L13806, <https://doi.org/10.1029/2005GL023109>, 2005.

10    Beyerle, G., Grunwaldt, L., Heise, S., Köhler, W., König, R., Michalak, G., Rothacher, M., Schmidt, T.,  
11    Wickert, J., Tapley, B. D., and Giesinger, B.: First results from the GPS atmosphere sounding  
12    experiment TOR aboard the TerraSAR-X satellite, *Atmospheric Chemistry & Physics*, 11, 6687–6699,  
13    <https://doi.org/10.5194/acp-11-6687-2011>, 2011.

14    Chipperfield, M. P., Multiannual simulations with a three-dimensional chemical transport model, *J.*  
15    *Geophys. Res.*, 104(D1), 1781–1805, doi:10.1029/98JD02597, 1999.

16    Cucurull, L., J. C. Derber, and R. J. Purser: A bending angle forward operator for global positioning  
17    system radio occultation measurements. *Journal of Geophysical Research: Atmospheres*, 118, 14-28.  
18    doi: 10.1029/2012JD017782, 2013.

19    Dee, D. P., Uppala, S. M., Simmons, A. J., Berrisford, P., Poli, P., Kobayashi, S., Andrae, U.,  
20    Balmaseda, M. A., Balsamo, G., Bauer, P., Bechtold, P., Beljaars, A. C. M., van de Berg, L., Bidlot, J.,  
21    Bormann, N., Delsol, C., Dragani, R., Fuentes, M., Geer, A. J., Haimberger, L., Healy, S. B., Hersbach,  
22    H., Hólm, E. V., Isaksen, L., Kållberg, P., Köhler, M., Matricardi, M., McNally, A. P., Monge-Sanz, B.  
23    M., Morcrette, J.-J., Park, B.-K., Peubey, C., de Rosnay, P., Tavolato, C., Thépaut, J.-N. and Vitart, F.:  
24    The ERA-Interim reanalysis: configuration and performance of the data assimilation system. *Q.J.R.*  
25    *Meteorol. Soc.*, 137: 553–597. doi: 10.1002/qj.828, 2011.

26    Durre, I., R. S. Vose, and D. B. Wuertz, Overview of the Integrated Global Radiosonde Archive, *J.*  
27    *Clim.*, 19(1), 53–68, doi:10.1175/JCLI3594.1, 2006.

28    Efron, B., and R. J. Tibshirani, An Introduction to the Bootstrap, 436 pp., Chapman and Hall, New York,  
29    1993.

30    Emanuel, K., S. Solomon, D. Folini, S. Davis, and C. Cagnazzo, Influence of Tropical Tropopause Layer  
31    Cooling on Atlantic Hurricane Activity. *J. Climate*, 26, 2288–2301, <https://doi.org/10.1175/JCLI-D-12-00242.1>, 2013.

33    Folkins, I., M. Lowenstein, J. Podolske, S. Oltmans, and M. Proffitt, A barrier to vertical mixing at  
34    14 km in the tropics: Evidence from ozonesondes and aircraft measurements, *J. Geophys. Res.*, 104,  
35    22095–22102, 1999.

36    Free, M., Seidel, D. J., Angell, J. K., Lanzante, J., Durre, I., and Peterson, T. C., Radiosonde  
37    Atmospheric Temperature Products for Assessing Climate (RATPAC): A new data set of large-area  
38    anomaly time series, *J. Geophys. Res.*, 110, D22101, doi:10.1029/2005JD006169, 2005

39    Fueglistaler S, Dessler A E, Dunkerton T J, et al., Tropical tropopause layer, *Rev. Geophys.*, 47,  
40    RG1004, doi:10.1029/2008RG000267, 2009.

1 Fueglistaler, S., Haynes, P. H., and Forster, P. M.: The annual cycle in lower stratospheric temperatures  
2 revisited, *Atmos. Chem. Phys.*, 11, 3701-3711, <https://doi.org/10.5194/acp-11-3701-2011>, 2011.

3 Fujiwara, M., Suzuki, J., Gettelman, A., Hegglin, M. I., Akiyoshi, H., and Shibata, K., Wave activity in  
4 the tropical tropopause layer in seven reanalysis and four chemistry climate model data sets, *J. Geophys.*  
5 *Res.*, 117, D12105, doi:10.1029/2011JD016808, 2012.

6 Fujiwara, M., Hibino, T., Mehta, S. K., Gray, L., Mitchell, D., and Anstey, J.: Global temperature  
7 response to the major volcanic eruptions in multiple reanalysis data sets, *Atmos. Chem. Phys.*, 15,  
8 13507-13518, <https://doi.org/10.5194/acp-15-13507-2015>, 2015.

9 Fujiwara, M., Wright, J. S., Manney, G. L., Gray, L. J., Anstey, J., Birner, T., Davis, S., Gerber, E. P.,  
10 Harvey, V. L., Hegglin, M. I., Homeyer, C. R., Knox, J. A., Krüger, K., Lambert, A., Long, C. S.,  
11 Martineau, P., Molod, A., Monge-Sanz, B. M., Santee, M. L., Tegtmeier, S., Chabriat, S., Tan, D. G.  
12 H., Jackson, D. R., Polavarapu, S., Compo, G. P., Dragani, R., Ebisuzaki, W., Harada, Y., Kobayashi,  
13 C., McCarty, W., Onogi, K., Pawson, S., Simmons, A., Wargan, K., Whitaker, J. S., and Zou, C.-Z.:  
14 Introduction to the SPARC Reanalysis Intercomparison Project (S-RIP) and overview of the reanalysis  
15 systems, *Atmos. Chem. Phys.*, 17, 1417-1452, <https://doi.org/10.5194/acp-17-1417-2017>, 2017.

16 Gelaro, R., W. McCarty, M.J. Suárez, R. Todling, A. Molod, L. Takacs, C.A. Randles, A. Darmenov,  
17 M.G. Bosilovich, R. Reichle, K. Wargan, L. Coy, R. Cullather, C. Draper, S. Akella, V. Buchard, A.  
18 Conaty, A.M. da Silva, W. Gu, G. Kim, R. Koster, R. Lucchesi, D. Merkova, J.E. Nielsen, G. Partyka,  
19 S. Pawson, W. Putman, M. Riendecker, S.D. Schubert, M. Sienkiewicz, and B. Zhao: The Modern-Era  
20 Retrospective Analysis for Research and Applications, Version 2 (MERRA-2). *J. Climate*, 30, 5419–  
21 5454, <https://doi.org/10.1175/JCLI-D-16-0758.1>, 2017.

22 Gettelman, A., M. L. Salby, and F. Sassi: Distribution and influence of convection in the tropical  
23 tropopause region. *J. Geophys. Res.*, 107, 4080, doi:10.1029/2001JD001048, 2002.

24 Gettelman, A., et al., Multimodel assessment of the upper troposphere and lower stratosphere: Tropics  
25 and global trends, *J. Geophys. Res.*, 115, D00M08, doi:10.1029/2009JD013638, 2010.

26 Global Modeling and Assimilation Office (GMAO), MERRA-2 inst6\_3d\_ana\_Nv: 3d,6-Hourly,  
27 Instantaneous, Model-Level, Analysis, Analyzed Meteorological Fields V5.12.4, Greenbelt, MD, USA,  
28 Goddard Earth Sciences Data and Information Services Center (GES DISC), Accessed: [1.1.2015],  
29 10.5067/IUUF4WB9FT4W, 2015.

30 Gorbunov, M. E., Benzon, H.-H., Jensen, A. S., Lohmann, M. S., and Nielsen, A. S.: Comparative  
31 analysis of radio occultation processing approaches based on Fourier integral operators, *Radio Science*,  
32 39, RS6004, <https://doi.org/10.1029/2003RS002916>, 2004.

33 Haimberger, L., Homogenization of Radiosonde Temperature Time Series Using Innovation Statistics.  
34 *J. Climate*, 20, 1377–1403, <https://doi.org/10.1175/JCLI4050.1>, 2007.

35 Haimberger, L., Tavolato, C., and Sperka, S.: Homogenization of the Global Radiosonde Temperature  
36 Dataset through Combined Comparison with Reanalysis Background Series and Neighboring Stations,  
37 *J. Climate*, 25, 8108–3131, <https://doi.org/10.1175/JCLI-D-11-00668.1>, 2012.

38 Hajj, G. A., Ao, C. O., Iijima, B. A., Kuang, D., Kursinski, E. R., Mannucci, A. J., Meehan, T. K.,  
39 Romans, L. J., de la Torre Juarez, M., and Yunck, T. P.: CHAMP and SAC-C atmospheric occultation  
40 results and intercomparisons, *Journal of Geophysical Research (Atmospheres)*, 109, D06 109,  
41 <https://doi.org/10.1029/2003JD003909>, 2004.

1 Hartmann, D. L., J. R. Holton, and Q. Fu: The heat balance of the tropical tropopause, cirrus, and  
2 stratospheric dehydration. *Geophys. Res. Lett.*, 28, 1969–1972, 2001

3 Hersbach, H., et al., Operational global reanalysis: progress, future directions and synergies with NWP,  
4 ERA Report Series, 27, 2018.

5 Highwood, E. J. and Hoskins, B. J., The tropical tropopause. *Q.J.R. Meteorol. Soc.*, 124: 1579-1604.  
6 doi:10.1002/qj.49712454911, 1998.

7 Ho, S.-p., Peng, L., and Vömel, H.: Characterization of the longterm radiosonde temperature biases in  
8 the upper troposphere and lower stratosphere using COSMIC and Metop-A/GRAS data from 2006 to  
9 2014, *Atmospheric Chemistry & Physics*, 17, 4493–4511, <https://doi.org/10.5194/acp-17-4493-2017>,  
10 2017.

11 Holton, J. R. and Gettelman, A.: Horizontal transport and the dehydration of the stratosphere, *Geophys.*  
12 *Res. Lett.*, 28, 2799–2802, 2001.

13 Kim, J. and S. Son: Tropical Cold-Point Tropopause: Climatology, Seasonal Cycle, and Intraseasonal  
14 Variability Derived from COSMIC GPS Radio Occultation Measurements. *J. Climate*, 25, 5343–5360,  
15 <https://doi.org/10.1175/JCLI-D-11-00554.1>, 2012.

16 Kim, Y.-H., Kiladis, G. N., Albers, J. R., Dias, J., Fujiwara, M., Anstey, J. A., Song, I.-S., Wright, C.  
17 J., Kawatani, Y., Lott, F., and Yoo, C.: Comparison of equatorial wave activity in the tropical tropopause  
18 layer and stratosphere represented in reanalyses, *Atmos. Chem. Phys. Discuss.*,  
19 <https://doi.org/10.5194/acp-2019-110>, in review, 2019.

20 Kistler, R., Collins, W., Saha, S., White, G., Woollen, J., Kalnay, E., Chelliah, M., Ebisuzaki, W., Kanamitsu,  
21 M., Kousky, V., van den Dool, H., Jenne, R., and Fiorino, M.: The NCEP–NCAR 50-year reanalysis: monthly  
22 means CD-ROM and documentation, *B. Am. Meteorol. Soc.*, 82, 247–267, 2001.

23 Kobayashi, S., Ota, Y., Harada, Y., Ebita, A., Moriya, M., Onoda, H., Onogi, K., Kamahori, H.,  
24 Kobayashi, C., Endo, H., Miyaoka, K., and Takahashi, K.: The JRA-55 reanalysis: general specifica-  
25 tions and basic characteristics, *J. Meteorol. Soc. Jpn.*, 93, 5–48, doi:10.2151/jmsj.2015-001, 2015.

26 Krüger, K., Tegtmeier, S., and Rex, M.: Long-term climatology of air mass transport through the  
27 Tropical Tropopause Layer (TTL) during NH winter, *Atmos. Chem. Phys.*, 8, 813-823,  
28 <https://doi.org/10.5194/acp-8-813-2008>, 2008.

29 Krüger, K., Tegtmeier, S., and Rex, M.: Variability of residence time in the Tropical Tropopause Layer  
30 during Northern Hemisphere winter, *Atmos. Chem. Phys.*, 9, 6717-6725, <https://doi.org/10.5194/acp-9-6717-2009>, 2009.

32 Kursinski, E. R., Hajj, G. A., Schofield, J. T., Linfield, R. P., and Hardy, K. R.: Observing Earth's  
33 atmosphere with radio occultation measurements using the Global Positioning System, *Journal of*  
34 *Geophysical Research: Atmospheres*, 102, 23 429–23 465, <https://doi.org/10.1029/97JD01569>, 1997.

35 Lawrence, Z. D., Manney, G. L., and Wargan, K.: Reanalysis intercomparisons of stratospheric polar  
36 processing diagnostics, *Atmos. Chem. Phys.*, 18, 13547-13579, <https://doi.org/10.5194/acp-18-13547-2018>, 2018.

38 Long, C. S., Fujiwara, M., Davis, S., Mitchell, D. M., and Wright, C. J.: Climatology and interannual  
39 variability of dynamic variables in multiple reanalyses evaluated by the SPARC Reanalysis

1 Intercomparison Project (S-RIP), *Atmos. Chem. Phys.*, 17, 14593-14629, <https://doi.org/10.5194/acp-17-14593-2017>, 2017.

3 Maycock, A.C., et al., Revisiting the mystery of stratospheric temperature trends. *Geophys. Res. Lett.*,  
4 doi:10.1029/2018GL078035, 2018.

5 Mote, P. W., Rosenlof, K. H., McIntyre, M. E., Carr, E. S., Gille, J. C., Holton, J. R., Kinnersley, J. S.,  
6 Pumphrey, H. C., Russell, J. M., and Waters, J. W.: An atmospheric tape recorder: The imprint of  
7 tropical tropopause temperatures on stratospheric water vapor, *J. Geophys. Res.*, 101(D2), 3989–4006,  
8 doi:10.1029/95JD03422, 1996.

9 Nash, J., Oakley, T., Vömel, H., and Li, W.: WMO intercomparison of high-quality radiosonde systems,  
10 Yangjiang, China, 12 July–3 August 2010, *Instruments and Observing Methods Report No. 107*,  
11 WMO/TD-No. 1580, WMO, Geneva, Switzerland, 238 pp., 2011.

12 Naujokat, B., An update of the observed quasi-biennial oscillation of the stratospheric winds over the tropics,  
13 *J. Atmos. Sci.*, 43, 1873-1877, 1986.

14 Nishimoto, E., and M. Shiotani, Seasonal and interannual variability in the temperature structure around  
15 the tropical tropopause and its relationship with convective activities, *J. Geophys. Res. Atmos.*, 117,  
16 D02104, doi:10.1029/2011JD016936, 2012.

17 Nishimoto, E., and M. Shiotani, Intraseasonal variations in the tropical tropopause temperature revealed  
18 by cluster analysis of convective activity, *J. Geophys. Res. Atmos.*, 118, 3545–3556, doi:  
19 10.1002/jgrd.50281, 2013.

20 Onogi, K., Tsutsui, J., Koide, H., Sakamoto, M., Kobayashi, S., Hat-sushika, H., Matsumoto, T.,  
21 Yamazaki, N., Kamahori, H., Taka-hashi, K., Kadokura, S., Wada, K., Kato, K., Oyama, R., Ose, T.,  
22 Mannoji, N., and Taira, R.: The JRA-25 reanalysis, *J. Meteorol. Soc. Jpn.*, 85, 369–432,  
23 doi:10.2151/jmsj.85.369, 2007.

24 Pan, L. L., and Munchak, L. A.: Relationship of cloud top to the tropopause and jet structure from  
25 CALIPSO data, *J. Geophys. Res.*, 116, D12201, doi:10.1029/2010JD015462, 2011.

26 Pan, L. L., Honomichl, S. B., Bui, T. V., Thornberry, T., Rollins, A., Hints, E., & Jensen, E. J.: Lapse  
27 Rate or Cold Point: The Tropical Tropopause Identified by In Situ Trace Gas Measurements.  
28 *Geophysical Research Letters*, 45(19), 10-756, 2018.

29 Randel W. J., and Jensen, E., Physical processes in the tropical tropopause layer and their roles in a  
30 changing climate. *Nat Geosci* 6:169–176, 2013.

31 Randel, W. J., F. Wu, and D. J. Gaffen, Low frequency variations of the tropical tropopause from NCEP  
32 reanalyses. *J. Geophys. Res.*, 105, 15 509–15 523, 2000.

33 Randel, W. J., F. Wu, S.J. Oltmans, K. Rosenlof, and G.E. Nedoluha, Interannual Changes of  
34 Stratospheric Water Vapor and Correlations with Tropical Tropopause Temperatures. *J. Atmos. Sci.*,  
35 61, 2133–2148, <https://doi.org/10.1175/1520-0469.2004a>, 2004a.

36 Randel, W. J., P. Udelhofen, E. Fleming, M. Geller, M. Gelman, K. Hamilton, D. Karoly, D. Ortland,  
37 S. Pawson, R. Swinbank, F. Wu, M. Baldwin, M. Chanin, P. Keckhut, K. Labitzke, E. Remsberg, A.  
38 Simmons, and D. Wu, The SPARC Intercomparison of Middle-Atmosphere Climatologies. *J. Climate*,  
39 17, 986–1003, [https://doi.org/10.1175/1520-0442\(2004\)017](https://doi.org/10.1175/1520-0442(2004)017), 2004b.

1 Randel, W. J., Shine, K. P., Austin, J., Barnett, J., Claud, C., Gillett, N. P., et al., An update of observed  
2 stratospheric temperature trends. *Journal of Geophysical Research*, 114, D02107.  
3 <https://doi.org/10.1029/2008JD010421>, 2009.

4 Rienecker, M. M., Suarez, M. J., Gelaro, R., Todling, R., Bacmeister, J., Liu, E., Bosilovich, M. G.,  
5 Schubert, S. D., Takacs, L., Kim, G.-K., Bloom, S., Chen, J., Collins, D., Conaty, A., da Silva, A., Gu,  
6 W., Joiner, J., Koster, R. D., Lucchesi, R., Molod, A., Owens, T., Pawson, S., Pegion, P., Redder, C. R.,  
7 Reichle, R., Robertson, F. R., Ruddick, A. G., Sienkiewicz, M., and Woollen, J.: MERRA: NASA's  
8 modern-era retrospective analysis for research and applications, *J. Climate*, 24, 3624–3648,  
9 doi:10.1175/JCLI-D-11-00015.1, 2011.

10 Saha, S., Moorthi, S., Pan, H.-L., Wu, X., Wang, J., Nadiga, S., Tripp, P., Kistler, R., Woollen, J.,  
11 Behringer, D., Liu, H., Stokes, D., Grumbine, R., Gayno, G., Wang, J., Hou, Y.-T., Chuang, H.-Y.,  
12 Juang, H.-M. H., Sela, J., Iredell, M., Treadon, R., Kleist, D., van Delst, P., Keyser, D., Derber, J., Ek,  
13 M., Meng, J., Wei, H., Yang, R., Lord, S., van den Dool, H., Kumar, A., Wang, W., Long, C., Chelliah,  
14 M., Xue, Y., Huang, B., Schemm, J.-K., Ebisuzaki, W., Lin, R., Xie, P., Chen, M., Zhou, S., Higgins,  
15 W., Zou, C.-Z., Liu, Q., Chen, Y., Han, Y., Cucurull, L., Reynolds, R. W., Rutledge, G., and Goldberg,  
16 M.: The NCEP climate forecast system reanalysis, *B. Am. Meteorol. Soc.*, 91, 1015–1057,  
17 doi:10.1175/2010BAMS3001.1, 2010.

18 Santer, B.D., R. Sausen, T.M.L. Wigley, J.S. Boyle, K. AchutaRao, C. Doutriaux, J.E. Hansen, G.A.  
19 Meehl, E. Roeckner, R. Ruedy, G. Schmidt, and K.E. Taylor, Behavior of tropopause height and  
20 atmospheric temperature in models, reanalyses, and observations: Decadal changes. *J. Geophys. Res.*,  
21 108, no. D1, 4002, doi:10.1029/2002JD002258, 2003.

22 Schoeberl, M. R., A. E. Dessler, and T. Wang., Simulation of stratospheric water vapor and trends using  
23 three reanalyses." *Atmospheric Chemistry and Physics*, 12 (14): 6475-6487 doi:10.5194/acp-12-6475-  
24 2012, 2012.

25 Seidel, D. J., and Randel, W. J., Variability and trends in the global tropopause estimated from  
26 radiosonde data, *J. Geophys. Res.*, 111, D21101, doi:10.1029/2006JD007363, 2006

27 Seidel, D. J., R. J. Ross, J. K. Angell, and G. C. Reid, Climatological characteristics of the tropical  
28 tropopause as revealed by radiosondes, *J. Geophys. Res.*, 106(D8), 7857–7878,  
29 doi:10.1029/2000JD900837, 2001.

30 Sherwood, S. C., T. Horinouchi, and H. A. Zelezniak: Convective impact on temperatures observed near  
31 the tropical tropopause. *J. Atmos. Sci.*, 60, 1847–1856, 2003.

32 Simmons, A. J., Poli, P., Dee, D. P., Berrisford, P., Hersbach, H., Kobayashi, S. and Peubey, C.,  
33 Estimating low-frequency variability and trends in atmospheric temperature using ERA-Interim. *Q.J.R.  
34 Meteorol. Soc.*, 140: 329-353. doi:10.1002/qj.2317, 2014.

35 Tao, M., Konopka, P., Ploeger, F., Yan, X., Wright, J. S., Diallo, M., Fueglistaler, S., and Riese, M.:  
36 Multitimescale variations in modeled stratospheric water vapor derived from three modern reanalysis  
37 products, *Atmos. Chem. Phys.*, 19, 6509–6534, <https://doi.org/10.5194/acp-19-6509-2019>, 2019.

38 Thorne, P. W., D. E. Parker, S. F. B. Tett, P. D. Jones, M. McCarthy, H. Coleman, and P. Brohan,  
39 Revisiting radiosonde upper air temperatures from 1958 to 2002, *J. Geophys. Res.*, 110, D18105,  
40 doi:10.1029/2004JD005753, 2005.

1 Thomason, L. W., Ernest, N., Millán, L., Rieger, L., Bourassa, A., Vernier, J.-P., Manney, G., Luo, B.,  
2 Arfeuille, F., and Peter, T.: A global space-based stratospheric aerosol climatology: 1979–2016, *Earth*  
3 *Syst. Sci. Data*, 10, 469–492, <https://doi.org/10.5194/essd-10-469-2018>, 2018.

4 von Engeln, A., Andres, Y., Marquardt, C., and Sancho, F.: GRAS radio occultation on-board of Metop,  
5 *Advances in Space Research*, 47, 336–347, <https://doi.org/10.1016/j.asr.2010.07.028>, 2011.

6 Wang, J. S., Seidel, D. J., and Free, M., How well do we know recent climate trends at the tropical  
7 tropopause?, *J. Geophys. Res.*, 117, D09118, doi:10.1029/2012JD017444, 2012.

8 Wheeler, M. and G.N. Kiladis, Convectively Coupled Equatorial Waves: Analysis of Clouds and  
9 Temperature in the Wavenumber–Frequency Domain. *J. Atmos. Sci.*, 56, 374–399,  
10 [https://doi.org/10.1175/1520-0469\(1999\)056<0374:CCEWAO>2.0.CO;2](https://doi.org/10.1175/1520-0469(1999)056<0374:CCEWAO>2.0.CO;2), 1999.

11 Wickert, J., Reigber, C., Beyerle, G., König, R., Marquardt, C., Schmidt, T., Grunwaldt, L., Galas, R.,  
12 Meehan, T. K., Melbourne, W. G., and Hocke, K.: Atmosphere sounding by GPS radio occultation: First  
13 results from CHAMP, *Geophysical Research Letters*, 28, 3263–3266,  
14 <https://doi.org/10.1029/2001GL013117>, 2001.

15 World Meteorological Organization: Definition of the tropopause, *Bulletin of the World Meteorological*  
16 *Organization*, 6, 136–137, 1957.

17 Wright, C. J. and Hindley, N. P.: How well do stratospheric reanalyses reproduce high-resolution satellite  
18 temperature measurements?, *Atmos. Chem. Phys.*, 18, 13703–13731, <https://doi.org/10.5194/acp-18-13703-2018>, 2018.

20 Xie, F., Li, J., Tian, W., Li, Y., & Feng, J., Indo-Pacific warm pool area expansion, Modoki activity,  
21 and tropical cold-point tropopause temperature variations. *Scientific reports*, 4, 4552.  
22 doi:10.1038/srep04552, 2014.

23 Zhou, X.L., M.A. Geller, and M.H. Zhang, Tropical Cold Point Tropopause Characteristics Derived  
24 from ECMWF Reanalyses and Soundings. *J. Climate*, 14, 1823–1838, <https://doi.org/10.1175/1520-0442.2001.014.0182.0442>, 2001.

26

27